Chapter 1
Introduction to Cavity Enhanced Absorption Spectroscopy

Daniele Romanini, Irène Ventrillard, Guillaume Méjean, Jérôme Morville, and Erik Kerstel

Abstract In this introductory chapter we will begin with an historical outline of the development of cavity enhanced absorption methods, with just enough attention to the applications that either motivated them or became conceivable after their development. Given the number of publications in this domain, we will consider only the first demonstrations, and those works leading to substantial improvement or innovation in the state of the art.

Subsequently, rather than reviewing in detail all principal applications, we will provide a review of the many reviews that have already appeared, even quite recently, dealing preferentially with a specific cavity enhanced implementation or a specific domain of application.

Finally, we will provide wide but mostly intuitive foundations for approaching to cavity enhanced methods, by considering first the physics behind the (static) response of a cavity in the spectral domain, followed by a discussion of the physics of the (transient) coupling of different types of lasers to a cavity, going from the ideal tunable monochromatic wave to the realistic noisy continuous wave laser, to the pulsed nanosecond laser, and finally the broadband femtosecond laser combs. We will try to situate the most widespread cavity enhanced schemes along these detailed discussions.

1.1 Introduction

Cavity Enhanced Absorption Spectroscopy (CEAS) is used in this book mostly in a broad sense, as including all absorption spectroscopic methods exploiting the principal property of high finesse optical cavities, which is the increase of the interaction time of light with matter. The narrow technical meaning of CEAS will be also used

D. Romanini (✉) · I. Ventrillard · G. Méjean · E. Kerstel
LIPhy UMR 5588, Univ. Grenoble 1/CNRS, 38041 Grenoble, France
e-mail: danielromanini@gmail.com

J. Morville
Institut Lumière Matière, UMR5306 Université Lyon 1-CNRS, Université de Lyon, 69622 Villeurbanne cedex, France

G. Gagliardi, H.-P. Loock (eds.), *Cavity-Enhanced Spectroscopy and Sensing*, Springer Series in Optical Sciences 179, DOI 10.1007/978-3-642-40003-2_1,

when talking about specific detection schemes in which the intracavity absorption is deduced from the intensity of light transmitted by the cavity (usually time averaged), as opposed to ring-down or phase-shift methods where the time dependence of transmitted light is used.

From a fundamental point of view, an optical cavity is first of all a resonator. Resonators have always been associated with sensitive measurements in physics, and are widely present in high-tech instrumentation and in everyday appliances. A common example is the radio tuner, in which an electronic resonator enhances a weak signal from a radio antenna at a specific frequency channel. The sensitivity and selectivity of the oscillation amplitude of a resonator to external perturbations at a specific frequency makes it analogous to a lock-in detection system. The response is notably characterized by an integration time given by the duration of the resonator oscillation after an impulsive excitation. Another property of resonators is to support stable resonance frequencies well determined by some physical parameters. Most modern watches exploit a narrow acoustic resonance of a quartz crystal as a stable reference that can be excited with little power (by an electronic oscillator with poor frequency stability) and enables the precise measurement of time. Temperature control of such a crystal may be used to stabilize its lattice spacing and stiffness and avoid drifts of the resonance frequency. Before electronics and quartz acoustic resonators, spring resonators were widely used for watches, and even earlier a pendulum oscillator, more adequate for clocks than wrist watches. In physics laboratories, electronic oscillations of isolated and cold atoms are used to measure time, and frequency, ever more precisely. Finally, a femtosecond light pulse oscillating inside a laser resonator generates an optical frequency comb, which is today the highest precision ruler available for comparing and linking widely separated optical frequencies.

Before the advent of optical cavities, absorption spectroscopy was hampered by the limited interaction length of the light beam through the sample, by amplitude fluctuations of the source, and by frequency fluctuations of the laser source in the case of the highest spectral resolution measurements (as needed for gas phase samples). Multiple-pass cells provided the most intuitive and appealing solution for increasing the interaction length, but their implementation turns out to be technically complex when hundreds of passes are desired. In particular, their challenging optical alignment requires highly stable mechanics. Large mirrors, and by consequence a large sample volume, are required in order to reduce the detrimental effects of optical interference between neighboring reflections. All the while, source amplitude and frequency noise persist and require an independent solution, further complicating the experimental setup. Optical cavities can provide a simultaneous solution for these different problems, as one can already understand from their general properties outlined above. The enhancement of the light-matter interaction time in a high finesse optical cavity may correspond to an effective interaction length of thousands of passes, and it turns out that increasing this interaction length by a still higher cavity finesse does not add to technical complexity (except for the fabrication of better mirrors). In addition, measurement of the cavity excitation decay (ring-down signal) gives access to the intracavity sample absorption regardless of amplitude source

fluctuations. Finally, cavity resonances may be put at work to provide a highly precise frequency scale, significantly improving on the intrinsic frequency stability of a laser source. An apparently smaller advantage, but fundamental for some applications, is that the sample size in a high finesse cavity is ultimately limited by the size of the $TEM_{0,0}$ mode, much smaller than the volume required by a multipass system.

1.1.1 A Short History of Cavity Enhanced Methods

Since Joseph von Fraunhofer demonstrated his first spectroscope in 1814, spectroscopy has been used in a bewildering range of studies in physics and chemistry. Given the broad scope of applications, the technical developments have naturally been pursued with widely different motivations, which is also true for CEAS. In this section we will attempt to sketch a wide panorama of developments that each time resulted in different methods of performing CEAS measurements (in its broad sense).

It is difficult to date the first documented theoretical or experimental demonstration concerning the use of optical cavities to enhance absorption measurements. As underlined above, resonators are present in everyday life and in physics laboratories, mostly due to their properties of frequency selectivity and stability. It was not coincidental that these properties of optical cavities were the first to be studied theoretically and to be exploited in the laboratory. Around 1961–1962, investigation of optical resonators focused on their spectral properties, and in particular on the existence of narrow transmission resonances associated with specific transverse field patterns [1, 2]. As noted by Jackson [3], in the earliest applications optical cavities made of flat mirrors (the original Fabry-Perot etalon) were indeed exploited for their spectral resolving power to deliver high resolution atomic spectra. But already in 1958, Connes had understood the advantages of using spherical concave mirrors for such applications and exposed the confocal cavity configuration [4] and its special properties. Jackson was probably the first to exploit a confocal cavity a couple of years later [3] to obtain cavity-filtered, and also cavity-enhanced, high-resolution spectra of electronic transitions in a beam of Barium atoms, using a spectral lamp as a source and a grating spectrometer for rough spectral selection.

In 1962 the first published issue of Applied Optics presented as a second contribution (p. 17) a paper titled "Atomes à l'intérieur d'un Interféromètre Perot-Fabry" [5] in which Albert Kastler clearly stated the potential interest of using an optical cavity for atomic spectroscopy. Among other relevant statements, the abstract reads: "*... the absorption of atoms inside the interferometer is studied. It is shown that this device is equivalent to a long absorption path in an ordinary light beam.*" (the rest of the paper is in French).

While more theoretical [6–9] and experimental [10, 11] insight was pursued, several years passed before new applications were stimulated by the manufacturing of dielectric mirrors with increasing reflectivity and lower losses, which also demanded special efforts to be characterized, and were going to provide optical cavities with

astonishing finesse several years later [12]. In 1977 Damaschini [13] proposed using a resonator with an intracavity Brewster plate for input and output coupling, and demonstrated reflectivity measurements with few parts per thousands accuracy by measuring the transmitted intensity. It was 1980 when Herbelin et al. [14] reported cavity photon lifetime measurements by the same phase-shift method previously applied to determine excited-state lifetimes in atoms and molecules by laser induced fluorescence. From the photon lifetime the mirror reflectivity could be accurately determined at the 100 ppm level. The idea is to modulate the amplitude of the excitation field and measure (by lock-in electronics) the phase shift of the induced modulation appearing at the cavity output, which is inversely proportional to the cavity photon lifetime. Herbelin et al. discussed the potential of measuring absorption also from gas or solid samples inserted in the cavity. The major limitation of the phase-shift measurement was the large fluctuations of the cavity injection level attributed to acoustic fluctuations of the cavity (but really due to laser phase noise), requiring long signal averaging. This scheme was later exploited again for CEAS [15, 16]. However, without locking of the laser frequency to the cavity resonance, it appears that excessive noise condemns this simple and appealing technique to a lower performance compared to other CEAS schemes.

Four years after Herberlin's paper, Anderson et al. [17] tackled the same problem by a direct measurement of the cavity photon lifetime with a sensitivity down to the 5 ppm level. In their words: "*Our technique relies on the fact that, with no light incident on the cavity, its output is determined only by its transient response which is characterized by an exponential decay of the intensity with a time constant which in turn is determined only by the round trip losses of the cavity, the round trip path length of the cavity, and the speed of light*". This is perhaps the first cavity ring-down application, accompanied by a clear statement of its specific advantages (insensitivity to source intensity fluctuations), which was theoretically investigated ten years earlier by Kastler [18]. In order to obtain the transient response, the accidental resonant cavity injection by a CW (continuous wave) laser was used, with a threshold detector on the cavity output signal triggering interruption of the injection by a fast electro-optic switch. As Anderson et al. observed (note 3 of [17]), the measurement of the decay time has its roots in electronics, in passive RCL circuit theory and microwave networks. They also discussed the theory of the cavity decay with a rigorous approach based on the light field rather than its intensity (the fast lane too often chosen by authors dealing with CEAS, see discussion in Sect. 1.2.1 around Eq. (1.12)). Using a bit of math, they pointed out a general property of resonators: The decay time reflects intrinsic resonator losses only if the excitation field is switched off fast enough. Other interesting points are acknowledged: When several transverse cavity modes are excited at a time, not only the beating of their frequencies may appear on the decay signal if the mode orthogonality is broken (as already shown by Goldsborough [10]), in addition the decay may become a sum of exponentials with slightly different time constants, due to spatial inhomogeneity of the mirrors surface. Finally, Anderson et al. considered that cavity length fluctuations could impact the measured decay time. But they did not give clear reasons as to why this effect remains negligible in practice. Luckily enough, photons trapped

in a cavity mode follow the changes of its resonance frequency all along the field decay, thanks to the Doppler frequency shift at reflection from a moving mirror [19].

The figurative term "cavity ring-down" was introduced only around 1985 by Crawford [20] to denote the exponential decay of the intracavity light intensity after impulsive excitation (or abrupt interruption of a continuous excitation). Like Anderson, Crawford et al. were developing accurate reflectance measurements, and they started using a pulsed dye laser to obtain cavity ring-down measurements over the broad laser tuning range. They discussed [20, 21] other advantages of using nanosecond laser pulses, notably that no frequency match is necessary since the pulse linewidth is broader than the cavity mode separation. It was 1988 when O'Keefe and Deacon [22] obtained the spectrum of a weak magnetic-dipole transition in atmospheric oxygen, using the experimental scheme of Crawford, in what is now commonly considered to be the first demonstration of Cavity Ring-Down Spectroscopy (CRDS). Incidentally, they adopted the same term of "cavity ring-down" used by Crawford.

The wide spectral coverage of pulsed lasers, extended to the IR and the UV regions of the spectrum by nonlinear techniques like frequency doubling, Raman shifting, and optical parametric conversion, combined perfectly with the indifference of CRDS to their large intensity fluctuations. This encouraged several groups to implement CRDS for various applications, like the spectroscopy of weak molecular overtone bands in the gas phase [23], of molecular clusters in supersonic jets (in the IR) [24, 25], or the measurement of trace concentrations of radicals in chemical reactors [26] or flames (in the UV) [27]. In order to avoid spectral filtering effects by cavity resonances when using spectrally narrow lasers, Meijer et al. [27] proposed exploiting multi-transverse-modes excitation. They experimentally illustrated this idea by comparing the results from different cavity lengths for which transverse modes are either grouped in widely spaced degenerate groups (confocal cavity), or dispersed to produce a quasi-continuum cavity transmission, especially when using a non optimized beam alignment, far from mode-matched.

Another common situation, when absorption lines are spectrally narrower than the laser pulse, was considered in detail [28] and recognized to generate multi-exponential decays due to different losses across the injected spectrum. However a simple approximation was used to show that the integrated absorption of spectral lines may still be correctly recovered in the limit of small absorptions, as was soon experimentally confirmed [29]. These results (and implicitly those in [27]) were contested on the basis of experiments in which no filtering effect was observed [24], but no mode matching, nor a confocal cavity configuration, had been considered. In contrast to these claims, efforts continued to be made towards understanding and avoiding artifacts appearing with multi-transverse-modes cavity excitation (mode beatings, multi-exponential decay) [30–32]. Eventually van Zee et al. [33] achieved shot-noise-limited performance by single cavity mode excitation with a frequency stabilized pulsed OPO laser, with excellent spectral resolution, but at the price of increased experimental complexity.

Meanwhile, multiple-quantum-wells (MQW) diode lasers had started shining CW narrow-line radiation, stabilized and tunable thanks to optical feedback from an

external or internal grating, respectively as External Cavity Diode Lasers (ECDL) or as Distributed Feed-Back (DFB) diode lasers. These affordable devices promoted the spreading of a CW-CRDS technique introduced by Romanini et al. in 1997 using a CW single-frequency dye laser [34] and not long thereafter using an ECDL [35, 36]. In this simple scheme the cavity length is modulated to induce the recurrent transient excitation of a single cavity mode passing through resonance with the laser line. When the incoming wave resonates and builds up enough intracavity field so that cavity transmission reaches a given threshold, like in Anderson's scheme, a fast acousto-optic switch interrupts the laser beam to produce a ring-down event. As new ideas are never really new, this scheme had been exploited ten years earlier [37] for measuring the absorption of thin films deposited directly on a mirror surface, but the fact of using it for high resolution gas phase spectroscopy did demand some innovation, in particular an electronic control of the cavity length to maintain the frequency dither of a cavity resonance centered around the laser frequency while this is tuned. This allows the optimal and exclusive excitation of $TEM_{0,0}$ cavity modes after the laser beam is at least partially mode matched to the cavity, delivering reproducible ring-down spectra over broad spectral ranges enabling the determination of broad-band absorption features [36], opening the way to a number of important applications. Another advantage is that the acquisition rate is only limited by the duration of the cavity ring-down [38], not by the (low) repetition rate of a pulsed laser.

In order to improve frequency precision in CW-CRDS, and following their developments with single-mode pulsed CRDS, Hodges et al. started in 2006 a frequency-stabilized CRDS (FS-CRDS) program based on precise cavity length control [39, 40] dedicated to the investigation of molecular line shapes of weak and isolated transitions, at the frontier with metrology and fundamental physics. On the other hand Giusfredi et al. [41] demonstrated kHz accuracy in CW-CRDS using frequency comb referencing. More exploratory works based on CW-CRDS, but which are of wider interest, include the studies by Huang and Lehmann about excess noise in CRDS from transverse modes coupled by mirror surface scattering [42], or from an insufficient extinction by the optical switch [43, 44], or still from mirror birefringence and polarization effects [45], and the exploration of coupled cavities resulting in the fast control of a cavity finesse by Courtois and Hodges [46].

It appeared rapidly that CW-CRDS is more adapted than its pulsed sibling for high resolution and high precision spectroscopy. For example, it readily delivered sub-Doppler absorption spectra in a supersonic slit-jet [35, 47, 48] with a noise level (2×10^{-10}/cm), better than the best pulsed-CRDS results [23, 33] even though still far away from the shot noise limit. The main drawback of CW lasers often is their relatively limited tuning range. However high-end ECDLs allow mode-hop-free tuning of 4–5 % of their central frequency, and a series of telecom-packaged DFB diode lasers is a convenient solution to cover a large fraction of the near-IR (from about 1.2 to 1.8 μm), since these fibered devices are easily interchangeable [49]. Other implementations were proposed, e.g. to simplify the setup by avoiding the optical switch [50] (by means of a fast resonance shift, as earlier proposed in another context [51]), to obtain CRDS spectra by fast laser sweeps [52] down to ms time

scales [53], to improve the data acquisition rate by frequency locking [38, 54], to increase the signal-to-noise level by heterodyne detection [55, 56] or by tight cavity locking and fast averaging [54] (with improved frequency precision). Finally, brute-force averaging of several CW-CRDS spectra over long time periods, was shown to yield white noise statistics all the way down to a record detection level of 5×10^{-13}/cm (with an extreme cavity finesse), with a potential dynamic range approaching 10^6 [57].

An interesting property of CW-CRDS is that high intracavity power can be exploited to observe non-linear effects such as two-photon transitions or the saturation of molecular transitions (e.g. sub-Doppler Lamb dips) [58]. In 2010 Giusfredi et al. [41] exploited saturation in the mid-IR to obtain the empty cavity (baseline) losses and the sample absorption by fitting a molecular transition saturation model to a single (averaged) ring-down profile, assuming saturation follows adiabatically the decaying intracavity power. Using a high-power frequency-stabilized difference-frequency laser, they managed to use this principle to subtract large (4 %) cavity loss fluctuations affecting their measurements, all the while correcting for the strong saturation and obtain the unsaturated spectral profile of very intense fundamental vibrational transitions of CO_2. It should be underlined that this is an unusual situation, since ring-down measurements have often been shown to be very stable and reproducible [36, 57, 59]. Soon after, the same group applied their treatment of saturation to the first CW-CRDS measurement of a radiocarbon labelled molecule, $^{14}CO_2$, detecting standard atmospheric levels around 1 ppt, with a 43 ppq detection limit [60]. For this result they averaged successive frequency scans to reach a noise level of $\sim 2 \times 10^{-11}$/cm in 1 hour (as deduced from Fig. 2 of [60], corresponding to $10^{-9}/\text{cm}/\sqrt{\text{Hz}}$). The appealing perspective is that CRDS will replace large and expensive high-energy accelerator mass-spectrometers for radiocarbon dating. It is also interesting to note that CW-CRDS is already at the core of high-accuracy commercial trace gas and isotope ratio analyzers.

The small size and low power requirement of diode lasers spawned a blooming of compact spectrometers for trace analysis *in situ*, exploiting multiple-pass cells or high finesse cavities. While the ECDL mechanism is rather sensitive to the environment, DFB diode lasers are robust and reliable, and their smaller tuning range is sufficient to monitor one or two molecules at a time. In addition, their size and cost make it easy and affordable to install more than one laser in the same compact setup, sharing the same absorption cell, and using, for example, a modulation frequency multiplexing scheme to observe two spectra simultaneously (as in [61], albeit in a multiple-pass arrangement) or using simple time-division multiplexing [62]. DFB diode lasers initially covered the near IR but have been extended up to 3.4 μm using GaSb MQW structures. Lead-salt diode lasers were available earlier to access stronger transitions even at longer wavelengths, but they were (and are) affected by several problems, like cryogenic operation, not quite single-frequency emission, and poor beam quality. Quantum Cascade Lasers (QCL) operating in the mid IR were introduced in 1994 and evolved over several years from multi-line cryogenic devices to room temperature, reliable, high-power, single-frequency emission lasers (with DFB structure).

All these lasers, perhaps with the exception of lead-salt diodes, were coupled to high finesse cavities, in particular using the "basic" CEAS (in its narrow sense) scheme in which a CW laser is scanned across the cavity modes and the cavity output intensity is recorded without going through any ring-down time determination. The first implementations [63, 64], which also received the name ICOS (Integrated Cavity Output Spectroscopy), were user-friendly but not generous in terms of performance. In particular, long signal averaging was needed to eliminate the cavity mode structure, even when coupling the laser beam to a dense bath of high order transverse cavity modes as previously done with pulsed lasers. However, Paul et al. [65] eventually realized that with large mirrors and strongly off-axis cavity excitation it is possible to obtain a structureless continuous cavity transmission. Papers describing this off-axis ICOS implementation were not keen on discussing the technical details leading to the excellent results reported, but a few years and publications later it appeared that specific cavity configurations with respect to mirror separation, curvature, and (stress induced) astigmatism were exploited [66, 67]. At least initially, only a few researchers appeared to master this seemingly simple technique, while others were not able to go beyond typical ICOS performance levels. Still, this technique was perhaps the first form of CEAS (in the narrow sense) to find its way into commercial trace gas and isotope ratio analyzers.

A similar story may be told with respect to the use of Optical Feedback (OF) to obtain optimal coupling of laser radiation into cavity resonances: A simple V-shape cavity geometry produces frequency selective OF from the resonant field inside the cavity. In a first implementation, long-pulse operation of a DFB diode laser was used to obtain ring-down events at the end each pulse, with poor frequency stability and no easy control to force the same cavity mode to ring-down at the end of each pulse [68, 69]. The fact that one or another cavity mode becomes excited at the end of the laser pulse depends on the OF phase, which in turn is sensitive to sub-wavelengths changes of the laser-cavity distance. Without a control over this phase, this OF-CRDS scheme delivers modest performance but is tolerant to misalignment and vibrations. Eventually, Morville et al. [70] introduced an OF-CEAS scheme based on a linear laser frequency sweep, which allowed to easily implement an active phase control and obtain the injection of all $TEM_{0,0}$ modes in the laser scan, reproducibly and with low noise. An important benefit is that an absorption spectrum is sampled at nearly perfectly equidistant steps in frequency space. OF-CEAS can thus deliver high quality spectra over relatively fast diode laser scans, several times per second, with a small sample volume (like most CEAS techniques, and unlike multipass cells and off-axis ICOS), which also enables sub-second sample exchange times. And this is possible with an optical layout almost as simple as that of a basic absorption spectroscopy setup. Still, this technique demands a good understanding of several physical details, and thus, so far, it is only exploited by few research groups for application to trace gas monitoring in different environments [71, 72], including breath analysis faster than a respiratory cycle [73], isotope ratio analyses [74], or aerosol measurements [75], where particle size distribution could be related to signal fluctuations. At the same time, the OF-CEAS scheme is still being further developed and tested [76–79], and may be exploited for applications other than spectroscopy, notably for the measurement of the Kerr effect in

gases at the shot-noise limited level of 10^{-13} radians [80]. Recently, OF-CEAS also started to appear in commercial trace gas analyzers.

Nonetheless, except for fast measurements, there appears to be no major performance benefit when using OF-CEAS over some competing CEAS techniques, but this may be expected to change with application of the technique in the mid IR. OF-CEAS has been shown to be compatible with QCLs [81, 82] and to attain high S/N even with room temperature photodetectors. This contrasts with other CEAS schemes or multiple-pass arrangements that require cooled detectors to compensate for the low signals levels and the decreasing sensitivity of detectors with wavelength.

To conclude with CEAS based on a single-frequency laser, the NICE-OHMS technique (Noise-Immune Cavity-Enhanced Optical Heterodyne Molecular Spectroscopy) introduced by Ye et al. [83] deserves a special mention, with its shot noise limited detection placing it several orders of magnitude above other CEAS implementations. The principle is to use high frequency phase modulation of the laser wave to obtain spectrally symmetric sidebands, with subsequent locking of the carrier and the sidebands to successive cavity modes and demodulation of the cavity output as in heterodyne spectroscopy: a small and narrow intracavity absorption line will then produce a displacement (by the associated dispersion) and/or attenuation, either of the carrier or of one sideband, sensitively detected as an unbalance and change in the heterodyne signal. Like other frequency modulation techniques, this scheme requires good knowledge of the modulation parameters in order to provide quantitative absorption measurements, with some modelling. In return it provided spectacular results in detecting the narrow sub-Doppler saturation dips of overtone transitions [83], down to a 10^{-14}/cm detection limit for 1 s averaging, performance never reproduced since. NICE-OHMS requires sophisticated RF electronics and includes several frequency locking loops. In addition, when considering application to Doppler limited spectroscopy and to trace analysis, it is eventually limited by optical interference fringes [84, 85], like other absorption techniques, as we discuss in Sect. 1.3. On the other hand, given the use of frequency locking, NICE OHMS is also well suited to the mid-IR spectral range where Taubman et al. [85] obtained similar performance with a QCL as demonstrated by OF-CEAS [81]. NICE-OHMS also allows highly sensitive and selective spectroscopy of ions in a plasma when coupled with velocity modulation [86]. Recent developments exploiting fibered optics yield simplification, improved robustness and compactness, while they promise improved performance [87, 88].

The requirement in some applications to monitor a large spectral range was a good motivation to try and couple broadband light sources into a high finesse cavity, with spectral resolution provided by a grating spectrometer (coupled with a CCD[1] detector array) or a Fourier-Transform (FT) spectrometer. This idea is as old as 1987, when Dasgupta et al. [89] tested a Fabry-Perot cavity to enhance absorption through liquid samples in a commercial spectrophotometer, but it was pursued with

[1]Charge Coupled Device, a linear or rectangular array of small detectors capable of converting photons into electrons which are accumulated into charge wells before readout

more determination later on, using pulsed (nanosecond) dye lasers by Scherer et al. [90] and Ball et al. [91], high intensity arc lamps by Fiedler et al. [92], LEDs by Ball et al. [93], as well as super-continuum fiber sources by Johnston et al. [94]. All these light sources have rather different characteristics when considering their spatial and temporal coherence.

While these initial demonstrations spawned several applications and variations on this theme, notably for sensitive absorption spectroscopy in liquids [95] or in thin films [96], broadband CEAS is clearly suitable and limited to obtain low resolution absorption profiles covering a broad spectral range. Pushing the spectral resolution means reducing the photon flux per spectral element to such low levels that one needs to integrate the signal over excessively long times, even when using a sensitive CCD detector. Besides, CCD detectors possess a limited number of pixels, thus increasing the resolution implies reducing the spectral window available during one acquisition. On the other hand, FT acquisition of broad band spectra does not suffer from this limitation, but is inherently less sensitive [97, 98] and requires that the spectrum and intensity of the source remain steady during the acquisition of an interferogram, which may take from seconds up to minutes at higher resolutions [93]. Supercontinuum sources with single transverse mode output, are interesting for attaining higher resolution as they allow for an optimized cavity injection by cavity mode matching. In addition, broad-band total-internal-reflection "mirrors" [94, 99, 100] have been introduced by Lehmann [101] to keep up with such broad sources, since normal dielectric mirrors cover 'only' 5 to 20 % of their central wavelength. We should mention that total internal reflection was also exploited to realize completely solid cavities to investigate absorption of the evanescent wave by samples deposited at the surface [102]. It may appear surprising that broad band pulsed dye lasers, with their high spectral density and well collimated beam were not developed further after the first encouraging demonstrations [90, 91]. This was probably due to their unstable spectral profile together with a poor and fluctuating beam profile [90].

Mode-locked femtosecond lasers are another class of broadband sources. A femtosecond pulse generated and maintained by nonlinear effects in a laser cavity produces a highly stable series of replicas at the cavity output. The periodicity of this pulse train corresponds, by the properties of the FT, to a spectrum containing frequencies that are harmonics (multiples) of the repetition rate. This comb-like emission can be matched to the comb of cavity transmission resonances for optimal broad-band cavity injection. In addition, mode-locked lasers have a Gaussian beam, thus transverse mode matching is possible, altogether allowing to push spectral resolution much harder than with the broadband sources previously considered. Even more than nanosecond pulsed lasers, femtosecond lasers can take advantage of nonlinear effects to access almost any spectral region from the mid-IR to the deep UV. Finally, the development of stabilized laser combs makes available a high accuracy frequency scale for spectroscopic measurements.

Matching a frequency comb to a cavity corresponds in the time domain to matching the cavity length to the pulse repetition rate, such that each pulse coincides with a previous one after an integer number N of cavity round trips. This results in the

buildup of an intracavity pulse, in a manner analogous to the buildup considered earlier in CW-CRDS, but now occurring simultaneously for all those comb teeth that coincide (one every N) with a cavity mode. For this collective behavior to result in coherent buildup, in the time domain the carrier wave inside the laser pulse envelope must be in phase with the carrier of the previous pulse. In practice however, a delay between carrier and envelope accumulates over time from a small mismatch in group and phase velocity (due to dispersion), and it is not possible to overlap carrier and envelope perfectly from a pulse to the next, resulting in a frustrated buildup. In the frequency domain this corresponds to a non-zero frequency offset f_0 of the laser comb, such that its frequencies are written as $f_n = n f_{\text{rep}} + f_0$ (see also Fig. 1.6). In order to obtain optimal pulse buildup, the offsets of the laser and cavity combs should be matched.[2] Cavity injection by a laser comb was exploited to obtain selection of one in every N modes and increase the laser comb spacing and repetition rate in 1999 [103] but without having a spectroscopic application in mind. The same year the corresponding time-domain concept of pulse stacking was applied using a free electron laser in the mid-IR [104] to increase cavity throughput and obtain CRDS spectra by the phase-shift method, but only at a single frequency at a time (using a monochromator).

A truly broadband demonstration of comb-based CEAS, using a mode-locked fs Ti:Sapphire laser, had to wait until 2002 when Gherman et al. [105] generalized the CW-CRDS injection scheme by using periodic passages through a global comb resonance (transient injection) to obtain CEAS spectra from a spectrograph coupled with a CCD array detector. The same group illustrated the interest of this "Mode-Locked CEAS" (ML-CEAS) for accessing the blue and near-UV range [106, 107] thanks to the efficient frequency doubling of short pulses. These pioneering works were followed in 2006 by a multiplexed CRDS demonstration by Thorpe et al. [108] in the same spectral region, using a broader Ti:Sapphire comb and a dispersion-compensated high-finesse cavity. Indeed, dispersion inside an optical cavity limits the spectral window over which comb teeth can simultaneously match and inject the non-uniformly spaced cavity modes. Using special mirrors can mitigate this problem and indeed allowed Thorpe et al. to obtain cavity injection of a large spectral window. Using a rotating mirror as in [90] and a fast optical switch they obtained spectrally dispersed ring-down profiles on a CCD matrix following a broad-band transient cavity injection. In practice, multiplexed ring-down was not pursued further given the difficulty of obtaining many spectral elements (only 340 pixels in the cited demonstration) and good signal levels from a single passage through resonance. In addition, the particular advantage of a ring-down scheme, namely its ability to eliminate localized amplitude fluctuations, is superfluous given the smooth and stable spectral envelope of laser combs. In fact, a couple of years later the same group implemented a two-dimensional spectral dispersion system integrating a Vir-

[2] A shift applies also to the cavity resonances due to dispersion by the mirrors and in the intracavity medium, see Eq. (1.27).

tually Imaged Phased Array[3] (VIPA) to obtain about 1k spectral elements using a direct CEAS scheme [109] and again transient cavity injection.

More recently, as commercial mode-locked laser systems become more rugged and compact, it has become possible to conceive comb-CEAS systems for field measurements. In 2012 Grilli et al. completed a transportable near-UV ML-CEAS spectrometer equipped with two high finesse cavities for the measurement of atmospheric radicals in two spectral windows, attaining the shot-noise limit from 10 ms up to 10 minutes integration times [98]. This led to ppqv (10^{-15} volume mixing ratio) detection limits [110] for strongly absorbing molecules like IO. This instrument has been deployed in Antarctica, where it performed atmospheric measurements under rough conditions during one month [111].

An interesting alternative detection scheme exploits "Vernier" spectral selection between cavity and laser combs adjusted to have slightly detuned mode spacings: In combination with a CCD matrix detector, and using high precision frequency comb locking, individual comb modes could be resolved by Gohle et al. [112], while soon thereafter Thorpe et al. [113] reported using Vernier cavity filtering with a single photodetector.

Another important innovation is dual-comb multi-heterodyne detection, proposed by Schiller in 2002 [114], and later demonstrated in the mid-IR by Keilmann et al. [115, 116]. Two laser combs of slightly different repetition rate are superposed and beat on a single fast photodetector to produce a compressed RF replica of the product of the comb spectral envelopes [117–119], since each pair of teeth (one from each comb) beat at a slightly shifted RF frequency with respect to neighboring pairs. For example Coddington et al. [117] applied this concept to ultrastable erbium-fiber near-IR combs, covering a spectrum of 15.5 THz with 155k spectral elements defined to 1 Hz accuracy. A tunable filter was used to enable piece-wise recording of 1 THz acquisition windows, thus avoiding problems with photodetector saturation and dynamic range limitations. This was followed in 2009 by the first demonstration of dual-comb CEAS by Bernhardt et al. [120]. Recently, Chandler et al. [121] demonstrated the heterodyne concept coupled with pulsed-CRDS, using two high finesse cavities injected by a single ns laser pulse. This promising approach has the advantage of a simple experimental setup with no frequency locking, allows single shot acquisition with time resolution below the ring-down time, and spectral resolution of the cavity modes.

In 2010, comb-CEAS was coupled by Kassi et al. [122] to a commercial FT spectrometer. Using a commercial Ti:Sapphire comb they achieved a fairly high resolution, but over a limited spectral range and with an acquisition time of several minutes, and far from shot noise performance. A broadly tunable mid-IR fs commercial OPO system was also shown to work well with FT detection [123]. Foltynowicz et al. [124] have largely improved on these results by using comb frequency locking and a home-made FT spectrometer to cover a larger spectral interval with a much higher spectral resolution, few seconds acquisition time, and a shot-noise limited detection.

[3] See footnote 10.

1.1.2 A Review of Reviews on CEAS Developments and Applications

By now, cavity-ring-down and, more in general, cavity-enhanced spectroscopy have been the subject of a fair number of reviews, notably those of Scherer et al. in 1997 [125], Wheeler et al. in 1998 [126], Berden et al. in 2000 [127] and again in 2002 [128], Paldus et al. [129], Mazurenka et al. [130] and Vallance [131] in 2005. Books on the subject have also been edited, in 1999 by Busch and Busch [132], in 2003 by Van Zee and Looney [133], and by Berden and Engeln in 2009 [134].

The pulsed-CRDS technique as demonstrated by O'Keefe and Deacon [22] was followed by a number of cavity based methods, some of which have already seen their own specialized reviews. In 2003, Ball and Jones [135] reviewed the combination of CRDS and broad-band light sources. In 2007, Wang [136] reviewed the use of CRDS with plasma sources of atoms and elemental isotopes. In 2008, Thorpe and Ye [113] reviewed the combination of CEAS and frequency combs generated by mode-locked femtosecond pulsed lasers, while Foltynowicz et al. [137] described the state of affairs concerning the highly sensitive but complex NICE-OHMS technique. In 2010 Alder et al. [138] published a rather complete review on frequency comb cavity enhanced developments and applications, followed one year later by a shorter presentation of different comb CEAS schemes by Foltynowicz et al. [139]. In their 2010 review of the application of Quantum Cascade Lasers in chemical physics, Curl et al. [140] devote one section to cavity enhanced measurements using QCLs. The same year Waechter et al. [141] reviewed the use of waveguide (fibre) CRDS for chemical sensing, while Schnippering et al. [142] have treated, in 2011, recent advances in evanescent wave cavity-enhanced spectroscopy. The same year Orr et al. [143] wrote about developments and applications of specific schemes for fast-sweep CRDS, and in 2012 Long et al. [144] reviewed all frequency-stabilized CRDS works. Standing alone, is the 2009 tutorial by Lehmann and Huang [145] covering fitting algorithms and all what concerns optimal ring-down signal processing.

Apart from the above reviews that deal primarily with the technical aspects of one or more implementations of cavity-based spectroscopic measurements, a fair number of reviews deal with a restricted field of application. Brown in 2003 [146], Sigrist et al. in 2008 [147], Fiddler et al. in 2009 [148] and Cui et al. in 2012 [149] all looked at the application of cavity-based techniques in trace gas detection, and atmospheric monitoring in particular, while Atkinson in 2003 [150] dealt specifically with applications of CRDS in environmental chemistry. The aforementioned book edited by Berden and Engeln [134] contains a number of chapters dedicated to applications of cavity-based techniques. Applications to the analysis of stable isotope ratios of the light elements were reviewed by Kerstel in 2004 [151] and Kerstel and Gianfrani in 2008 [152]. In 2006, Loock [153] resumed the applications of fiber-based CRDS to microdevices for analysis of liquids. Cheskis and Goldman [154] reviewed in 2009 cavity ring-down spectroscopy of flames, whereas in the same year Wang and Sahay [155] reviewed the use of cavity enhanced techniques for exhaled breath analysis. The use of CRDS to measure the optical properties of aerosols

has been the subject of a critical discussion by Miles et al. in 2011 [156]. In their recent review on explosives detection Caygill et al. [157] briefly discuss the role of CRDS.

As the above mentioned reviews already demonstrate, cavity-based techniques have been applied to measure atomic and molecular absorption in the gas, liquid, and solid phases. Furthermore, these techniques make it possible to measure the total extinction due to the combined absorption and scattering by small particles (aerosols) inside the optical cavity. An empty cavity may also be configured to measure mirror reflectivity, and other parameters such as mirrors or sample linear or circular birefringence by detecting the change of polarization state of light transmitted by the cavity. Finally, fiber-based cavities can be used as sensitive miniature strain, acceleration and temperature sensors [158].

Of the many different possible applications, the measurement of the absolute absorption of infrared light by small molecules of environmental and health interests is certainly the most widespread, as it enables trace gas detection in, for example, atmospheric sciences, industrial monitoring, and biomedical research.

We will not attempt here to review all recent results which escaped the reviews cited above, also considering that these should be mostly covered in the following chapters of this book, treating many, if not all, domains of cavity-enhanced application.

It is worthwhile, however, to mention the still fairly recent commercial developments that have led to an explosion of the use of CEAS-equipped instrumentation in measuring (trace) gas concentrations and stable isotope ratios in applications ranging from (Ant)arctic ice-cores and climate research to ecosystem monitoring, carbon sequestration, and land-atmosphere surface exchange of greenhouse gases, and even qualification of ultrapure process gases. There are currently at least four commercial players that offer instruments based on CEAS techniques for the detection of small molecules of environmental and industrial interest, including H_2O, CO_2, N_2O, CO, CH_4, HF, HCl, C_2H_2, H_2S, NH_3, SO_2, OCS, and more, plus H_2O, CO_2, and CH_4 isotopes. Los Gatos Inc. of Mountain View (CA) builds instruments based on off-axis ICOS, while Tiger Optics of Warrington (PA) and Picarro of Santa Clara (CA) both rely on an implementation of CRDS. The French company AP2E of Aix-en-Provence uses the OF-CEAS technique in its trace gas analyzers.

This new generation of diagnostic tools for trace gas and isotope analyses provides high time resolution, high accuracy and precision, and can overcome limitations of more conventional instrumentation (such as gas chromatography or mass spectrometry) relating to robustness, portability, and cost of acquisition and ownership. Therewith they enable new laboratory and field applications of environmental and geochemical interest that in the past were difficult or impossible to carry out. Progress in this field is still rapid, resulting in improved instrument capabilities and an ever-widening range of applications. As a critical note, we mention that the affordability of these instruments and their acceptance by a fast growing class of users that is not necessarily aware of their working details may lead to concerns about calibration, validation, and data integrity.

1.2 The High Finesse Optical Resonator

CEAS and CRDS techniques are based upon the use of optical cavities in order to enhance light interaction with matter present inside the cavity, or even placed on the mirrors. An optical cavity is also referred to as an optical resonator, since the electromagnetic field inside the cavity becomes excited (and increases in amplitude) by incident light at some specific (resonant) frequencies. For simplicity we will initially consider cavity resonances associated with the cavity fundamental transverse mode, which are also referred to as longitudinal modes. We will see that these are uniformly separated in frequency space by the cavity Free Spectral Range which is the reciprocal of the round trip time: $\mathrm{FSR} = c/(2n_\mathrm{r}L_\mathrm{c}) = t_r^{-1}$, where $2L_\mathrm{c}$ is the cavity round trip length, c is the speed of light,[4] and n_r the index of refraction of the intracavity medium (a gas sample, usually). Another important cavity parameter, or actually a common figure of merit, is the finesse $\mathcal{F}$, defined by the ratio of the FSR over the full width at half maximum (FWHM) of the cavity resonances $\Delta\nu_\mathrm{c}$, for which a simple expression (for a symmetric 2-mirrors cavity) will be derived below. Sometimes the quality factor $\mathcal{Q}$ (also defined below) is used, given by the resonance frequency over its linewidth, which is equivalent (apart from a 2π factor) to consider the field energy stored at resonance over the energy fraction lost per optical cycle.

In the following, we will first derive the cavity transmission as a function of frequency yielding the longitudinal modes, then we will include the absorption by an intra-cavity sample. We will show that the effective absorption length is enhanced by a factor close to $\mathcal{F}$. Afterwards, we will give a brief introduction to transverse modes, allowing for a more realistic picture of the ways a cavity may be excited by an incident field. Indeed a cavity admits different families of resonances with specific transverse $TEM_{m,n}$ field distributions, where *TEM* stands for Transverse Electro-Magnetic and m, n are positive integers, and $TEM_{0,0}$ is the fundamental transverse mode [159].

1.2.1 Intensity Transmitted by a Cavity: A Simplified One-Dimensional Model

As previously mentioned, we consider a symmetric linear cavity made of two mirrors facing each other at a distance L_c along an optical axis z. Let us suppose an incoming monochromatic field with a Gaussian profile $E_0(x, y, z)$ in the transverse directions x, y:

$$E_\mathrm{in}(x, y, z, t) = E_0(x, y, z)\, e^{i(\omega t - kz)}.$$

We suppose that this Gaussian beam is mode-matched to the cavity, i.e. it matches in size and waist position the Gaussian profile of the $TEM_{0,0}$ mode. Transverse cavity

[4] ... or the light group velocity at the given optical frequency, if intracavity dispersion effects are considered.

modes $TEM_{m,n}$ are eigenfunctions of the cavity propagation operator [159], which means they are unchanged after propagating one round trip inside the cavity, except for a small intensity loss (and a phase shift dependent on the optical frequency and on m, n, which we will neglect for now). Thanks to this property, we can write the field transmitted by an empty cavity E_{out} by considering all cavity round trips ($z > L_c$, if we take the origin $z = 0$ at cavity input):

$$E_{\text{out}} = E_0(x, y, z) \sum_{p=0}^{\infty} \mathbf{t}^2 \mathbf{r}^{2p} e^{i\omega(t-2pL_c/c-L_c/c)-ikz}$$

$$= \frac{\mathbf{t}^2 e^{-i\omega L_c/c}}{1 - \mathbf{r}^2 e^{-i\omega t_r}} E_{\text{in}}(x, y, z, t), \tag{1.1}$$

where $\mathbf{t}$ and $\mathbf{r}$ are, respectively, the field transmission and the reflection coefficient of the two (equal) cavity mirrors, whose square modulus yield the corresponding coefficients for the light intensity $\mathcal{T}$ and $\mathcal{R}$. The case of an asymmetric cavity with different mirrors (with $\mathbf{r}_1, \mathbf{r}_2$ and $\mathbf{t}_1, \mathbf{t}_2$) is easily seen to give the same expressions below if we define $\mathcal{R} = \sqrt{\mathbf{r}_1 \mathbf{r}_2}$ and $\mathcal{T} = \sqrt{\mathbf{t}_1 \mathbf{t}_2}$. The term $i\omega(t - 2pL_c/c - L_c/c)$ is the phase change after one passage L_c/c plus p round trips. Taking the square absolute value leads directly to the transmitted intensity, the well-known Airy formula, expressing the comb of resonances uniformly spaced by the FSR:

$$I_{\text{out}}(\omega) = \frac{\mathcal{T}^2}{|1 - \mathcal{R} e^{-i\omega t_r}|^2} I_{\text{in}}$$

$$= \frac{\mathcal{T}^2}{(1-\mathcal{R})^2} \frac{I_{\text{in}}}{1 + (\frac{2\sqrt{\mathcal{R}}}{1-\mathcal{R}})^2 \sin^2(\omega t_r/2)}. \tag{1.2}$$

It should be noted that this single frequency development can be extended easily to any time dependent input field (still mode matched, for simplicity), by considering its Fourier expansion, which is a sum (or integral) of monochromatic waves with complex amplitude coefficients, and taking the cavity response to each of these. The superposition of all the cavity responses gives the complete time dependent cavity output, according to the superposition principle of linear response systems [30]. While the present description is a static one where the monochromatic wave is infinite in space and time, a more intuitive representation of the intracavity field building up from a wave, which is switched on at a given instant in time, will be presented in Sect. 1.4.1.

Around a resonant frequency, the transmitted intensity given by Eq. (1.2) is well approximated by a Lorentzian function. The FWHM of this resonance, and the cavity finesse, are:

$$\Delta\nu_c = \frac{1}{\pi t_r} \frac{1-\mathcal{R}}{\sqrt{\mathcal{R}}}, \tag{1.3}$$

$$\mathcal{F} = \frac{\text{FSR}}{\Delta\nu_c} = \pi \frac{\sqrt{\mathcal{R}}}{1-\mathcal{R}}. \tag{1.4}$$

The quality factor defined earlier turns out to be expressed in the following form:

$$\mathcal{Q} = \frac{\nu}{\mathrm{FSR}}\,\mathcal{F}, \tag{1.5}$$

where ν is the optical frequency of excitation.

As expected, the higher the reflectivity of the mirrors, the narrower the cavity modes and the higher the cavity finesse. Furthermore, we can derive the relation between $\Delta\nu_\mathrm{c}$ and the photon lifetime in the cavity, the ring-down time τ_RD. This is mathematically obtained by considering the cavity time response to an impulsive excitation which is written as the convolution of the pulse time profile and the FT of Eq. (1.1) taken for $r \sim 1$. Taking a delta function for the pulse, we obtain a decaying exponential for the field. Switching to the intensity ($I = |E|^2$), the decay becomes twice as fast and we find that the ring-down time is inversely proportional to the cavity mode width (which is related to the time-frequency uncertainty relation of FT theory):

$$\tau_\mathrm{RD} = \frac{1}{2\pi\,\Delta\nu_\mathrm{c}} = \frac{L_\mathrm{c}}{c}\,\frac{\sqrt{\mathcal{R}}}{1-\mathcal{R}}. \tag{1.6}$$

We see that the ring-down time is proportional to cavity finesse and to cavity length. It should be noted that a direct derivation of the ring-down time, by considering the cavity losses per round trip, yields the same result except for the term $\sqrt{\mathcal{R}}$, which is missing. With respect to high finesse cavities, these formulas are practically equivalent ($\mathcal{R} \simeq 1$). However, the first expression has the advantage of correctly going to zero in the limit $\mathcal{R} = 0$.

If we want now to include intracavity absorption in the previous treatment, we may consider that for each passage in the cavity the field is attenuated by the Lambert-Beer absorption factor $\exp(-\alpha L_\mathrm{c}/2)$, where α is the absorption coefficient and the factor $1/2$ comes from considering the field rather than the intensity (we neglect the imaginary part corresponding to dispersion and related to the absorption through the Kramers-Kronig relations [160]). At each passage in the cavity, light goes once through the sample and is reflected once by a mirror, we then see that the intra-cavity absorption factor can be associated to the mirror reflection coefficient. Additionally, to be exact we have to consider that the incoming light, which is directly transmitted by both mirrors at the first passage through the cavity, experiences intra-cavity absorption on the cavity length, which gives a global multiplicative factor of $\exp(-\alpha L_\mathrm{c}/2)$ on the cavity transmitted field. Then, we do not need to repeat the previous derivation but just apply these substitutions:

$$\begin{aligned} &\mathbf{r} \to \mathbf{r}\,e^{-\alpha L_\mathrm{c}/2} \quad \text{or} \quad \mathcal{R} \to \mathcal{R}\,e^{-\alpha L_\mathrm{c}} \\ &\text{and} \quad \mathbf{t}^2 \to \mathbf{t}^2 e^{-\alpha L_\mathrm{c}/2} \quad \text{or} \quad \mathcal{T}^2 \to \mathcal{T}^2 e^{-\alpha L_\mathrm{c}}. \end{aligned} \tag{1.7}$$

At resonance, when the optical frequency equals ω_q for the qth longitudinal mode, the phase $\omega_q t_r$ is a multiple[5] of 2π. From Eq. (1.2), we can thus write the

[5] We neglect here phase factors associated to the complex coefficients $\mathbf{r}$ and $\mathbf{t}$, which would introduce a tiny change of the effective cavity length. Likewise, we neglect the index of refraction n_r of

cavity transmission at resonance ω_q:

$$I_{\text{out}}(\omega_q) = I_{\text{in}}(\omega_q)\frac{\mathcal{T}^2\, e^{-\alpha L_c}}{(1-\mathcal{R}e^{-\alpha L_c})^2} \tag{1.8}$$

$$\simeq I_{\text{in}}(\omega_q) \times 1, \tag{1.9}$$

where the last passage is true for vanishing intracavity sample absorption and if mirror losses are negligible so that $\mathcal{T}+\mathcal{R} \simeq 1$. This is a well-known property of optical cavities made of two identical mirrors with equal $\mathcal{T}$ and equal $\mathcal{R}$: Cavity transmission at resonance may approach 100 % if total cavity losses are much smaller than mirror transmission.

It is interesting to compare this result to the simplified picture that is all too often encountered in the literature. This considers just the sum of the decreasing intensities over cavity round trips, instead of the corresponding amplitudes as was done here, yielding:

$$I_{\text{out}}(\omega_q) = I_{\text{in}}(\omega_q)\mathcal{T}^2 \sum_p \mathcal{R}^{2p} \tag{1.10}$$

$$= I_{\text{in}}(\omega_q)\frac{\mathcal{T}^2}{1-\mathcal{R}^2} \tag{1.11}$$

$$\simeq I_{\text{in}}(\omega_q) \times \frac{\mathcal{T}}{2}. \tag{1.12}$$

This result is clearly inconsistent with Eq. (1.9), which underlines the fact that field interference cannot be neglected, even when considering cavity response at resonance when the round trip phase is a multiple of 2π and field amplitudes simply add in phase. Mathematically it is evident that considering a round trip sum of intensities corresponds to dropping all crossed field terms:

$$\left|\sum_p \mathbf{r}^{2p}\right|^2 = \sum_{p,m} \mathbf{r}^{2p}\bar{\mathbf{r}}^{2m} \tag{1.13}$$

$$= \sum_p \mathcal{R}^{2p} + \left(\sum_{p\neq m} \mathcal{R}^p \mathcal{R}^m\right), \tag{1.14}$$

which is why a smaller cavity transmission is obtained.

The $\mathcal{T}/2$ loss of incident light resulting from this simplistic estimation is actually realized when using a broadband source or a swept laser (as we will see), which may justify that the crossed field terms average to zero as they correspond to the interference of incoherent fields. A simple picture allowing to better understand this situation, is that of an isolated and spectrally broad pulse, shorter than the cavity

the sample, which makes the cavity length equal to $n_r L_c$. These effects have no importance here, but they have an impact on cavity dispersion (spectral dependence of FSR, considered later).

round trip time. This pulse suffers an initial attenuation $\mathcal{T}$ when transmitted inside the cavity through the input mirror. Then, if we neglect losses, this fraction $\mathcal{T}$ of the pulse energy remains trapped in the cavity and will completely leak out of it in time, half in the forward and half in the backward direction, which accounts for the factor $1/2$. In the case of an incoherent LED or lamp, the source emission may be considered equivalent to a continuous sequence of short and broad pulses with random relative phases. The duration of these idealized pulses should be taken to correspond to the very short coherence time of the source, which may be proportional to the inverse of the emitted spectral width. While these hand-waving arguments seem reasonable, it is difficult to formalize them in a rigorous mathematical development in the time domain, while it is not particularly hard to obtain a rigorous analytical result by considering the frequency domain cavity response, as presented further down.

Let us now discuss the enhancement of intracavity absorption. From the cavity transmission at resonance Eq. (1.8), one obtains to first order in α:

$$\frac{I_{\text{out}}(\omega_q)}{I_{\text{in}}} \sim \frac{\mathcal{T}^2}{(1-\mathcal{R})^2}\left(1-\frac{2\alpha L_{\text{c}}}{1-\mathcal{R}}\right) \tag{1.15}$$

$$= \frac{\mathcal{T}^2}{(1-\mathcal{R})^2}\left(1-\alpha L_{\text{eff}}^{\text{res}}\right), \tag{1.16}$$

which holds if $\alpha L_{\text{c}} \ll 1-\mathcal{R}$. For a high finesse cavity, with typically $1-\mathcal{R} \sim 10^{-4}$, this would imply an absorption coefficient below 10^{-7} cm^{-1} (for $L_{\text{c}} \sim 1$ m). We see that for $\alpha \to 0$, the transmission approaches $\mathcal{T}^2/(1-\mathcal{R})^2$, which is close to unity for "low loss" mirrors (with $1-\mathcal{R} \simeq \mathcal{T}$). In practice, cavity transmission will be smaller than this if the laser linewidth is broader than the cavity resonance, and additionally if mode-matching is not perfect, as the incoming beam will only partially overlap with the $TEM_{0,0}$ mode being considered.

In Eq. (1.16), we introduced the effective absorption length where the cavity enhancement effect appears explicitly:

$$L_{\text{eff}}^{\text{res}} = \frac{2}{1-\mathcal{R}}\,L_{\text{c}} \simeq \frac{2\mathcal{F}}{\pi}\,L_{\text{c}}. \tag{1.17}$$

As expected using a resonant cavity, the absorption path length is enhanced by a large factor close to $\mathcal{F}$, as compared to a single pass over the sample length L_{c}. For a cavity finesse of 10^4, easily available in the visible and near-IR regions, and a cavity length of 1 m, the effective absorption length is already close to 10 km.

We should stress that this $2\mathcal{F}/\pi$ enhancement factor is only realized with a sufficiently monochromatic source probing the maximum of the cavity mode, which requires that a laser source is actively locked to a cavity resonance. In fact, the lock should be so "tight" that the laser frequency noise is reduced down to an emission linewidth well below the cavity mode width (more about this in Sect. 1.4.1).

In the opposite regime, with a broadband source such as a LED or a lamp, a lower enhancement factor is found [161]. To see this, let us consider Eq. (1.2) giving the

cavity transmission spectrum when multiplied by the source spectral power density. If we integrate this over a spectral window we obtain the total power transmitted in that window. Since a broad-band source has a smooth spectrum, we may consider it as constant if we take a sufficiently small window, for instance one cavity FSR. We are then left with the transmission function averaged over one FSR [161], yielding:

$$\mathcal{A} = \frac{1}{\mathrm{FSR}} \int_0^{\mathrm{FSR}} I_{\mathrm{out}}(2\pi\nu)\, d\nu = \frac{\mathcal{T}^2}{1-\mathcal{R}^2}\, I_{\mathrm{in}}, \tag{1.18}$$

where I_{out} has been substituted according to the Airy formula Eq. (1.2). Taking into account the absorption via the substitutions of Eqs. (1.7), we obtain:

$$\begin{aligned} \mathcal{A} &= \frac{\mathcal{T}^2 \exp(-\alpha L_{\mathrm{c}})}{1-\mathcal{R}^2 \exp(-2\alpha L_{\mathrm{c}})}\, I_{\mathrm{in}} \qquad (1.19) \\ &\simeq \frac{\mathcal{T}^2}{(1-\mathcal{R}^2)} \left(1 - \alpha \frac{L_{\mathrm{c}}}{1-\mathcal{R}}\right) I_{\mathrm{in}} \\ &\simeq \frac{\mathcal{T}}{2} \left(1 - \alpha L_{\mathrm{eff}}^{\mathrm{BB}}\right) I_{\mathrm{in}}, \qquad (1.20) \end{aligned}$$

where again we assume small absorption losses ($\alpha L_{\mathrm{c}} \ll 1-\mathcal{R}$) and high reflectivity mirrors ($\mathcal{R} \lesssim 1$). This confirms the previous non-rigorous result Eq. (1.12) that in broadband CEAS (BB-CEAS) the transmitted intensity is reduced by a factor $\mathcal{T}/2$ as compared to resonant CEAS. Additionally, we learn that the effective broadband absorption length $L_{\mathrm{eff}}^{\mathrm{BB}}$ is reduced by a factor 2:

$$L_{\mathrm{eff}}^{\mathrm{BB}} = \frac{1}{1-\mathcal{R}}\, L_{\mathrm{c}} \simeq \frac{\mathcal{F}}{\pi}\, L_{\mathrm{c}} = \frac{L_{\mathrm{eff}}^{\mathrm{res}}}{2}. \tag{1.21}$$

This difference in cavity enhancement comes from the fact that BB-CEAS is sensitive to the resonance profile surface, while resonant CEAS depends only on the peak transmission. When intra-cavity losses increase, the peak amplitude decreases faster than the mode profile area, because at the same time the width of the resonance increases (half as fast), as is easily verified.

The previous path-length enhancement factors are valid for cavity enhanced schemes, where the cavity output intensity is measured while the cavity is coupled with the light source. It is interesting to consider the ring-down case, where the cavity is isolated from the source during the measurement of the light decay time. It is then possible to define an effective path length as:

$$L_{\mathrm{eff}}^{\mathrm{RD}} = c\, \tau_{\mathrm{RD}} = \frac{\mathcal{F}}{\pi} L_{\mathrm{c}}, \tag{1.22}$$

equal to the path length for BB-CEAS. This is consistent with the fact that the decaying ring-down field is not composed only of photons sitting at the center of the resonance, which would require a longer observation time. It rather has the same spectral profile as the cavity mode, and the same as in BB-CEAS at cavity output. One can

also consider the first order expansion of τ_{RD} for small absorptions $\delta\alpha$, which is done by substituting Eqs. (1.7) inside Eq. (1.6). This yields $\delta\tau_{RD}/\tau_{RD} = L_{eff}^{RD}\delta\alpha$, as suggested for example by Thorpe et al. [113]. They also explain that in resonant cavity enhanced the backward wave is cancelled by interference with the directly reflected fraction of the input wave, compared with the ringdown case where light escapes from the cavity in both directions, accounting for a reduced sample interaction and two time smaller enhancement effect. This explanation does not seem to hold if we consider that in the resonant case reflection is null only in case the cavity has no losses (only mirror transmission) or its mirrors are chosen to satisfy an impedance matching condition (the input mirror transmission is equal to the sum of all other cavity losses and transmissions), however the enhancement factors derived above do not depend on this detail but only on the cavity finesse, thus the ratio of the enhancement factors for resonant cavity enhanced and CRDS is always 2.

The take-home message is that the enhancement factor in CEAS does not depend only on the cavity but also on the light source and the injection scheme. We have studied here static configurations in the two extreme limits where analytical results are straightforward, and in general we may write the enhancement factor as $\beta\mathcal{F}/\pi$ [113, 138], where β is a constant ranging between 1 for BB-CEAS and 2 for monochromatic resonant CEAS. We should also stress that the whole dependence on intracavity absorption is modified, since the absorption law for BB-CEAS Eq. (1.19) and resonant CEAS Eq. (1.8) are definitely not the same (see below and Fig. 1.1). In practice, intermediate configurations may exist but are not common. An interesting case is CEAS with a laser frequency locked to resonance, but not tightly enough to reduce its linewidth below that of the resonance (e.g. [124]). The average intensity transmitted will then be sensitive to the distribution of the laser spectrum across the resonance profile, which changes both in width and peak transmission as a function of cavity loss. This case will thus produce an intermediate β value that will vary when adjusting the locking loop. Even worse, the absorption law in this case will also be intermediate between that for the BB-CEAS and resonant CEAS, and will depend on the laser lineshape. Contrary to what claimed in [113, 138], β does not really depend on the laser tuning speed when transient injection schemes are concerned, except in a limit of very slow tuning, which is never realized in practice. Let us discuss this case in some detail.

If we take a transient injection with an ideal monochromatic wave tuning across resonance sufficiently slow that a complete cavity buildup is achieved, the transmitted peak will indeed present a sensitivity to cavity losses corresponding to $\beta = 2$. As the tuning speed will increase, the transmission profile will become distorted as discussed in Sect. 1.4.2, the peak intensity will decrease and the enhancement factor might start to decrease. However, there are two points to be considered. First of all, this is an extreme situation demanding a prohibitively slow tuning when we consider the response time and the mode width of a typical high finesse cavity.[6] Second, in swept CEAS schemes one does not consider the peak transmission, but some kind

[6]Inferior to 10 kHz/10 μs for a typical high finesse cavity, or about 0.1 s for tuning over one cavity FSR.

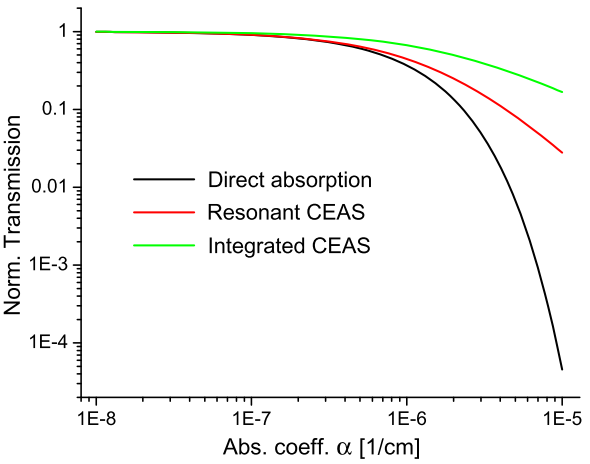

Fig. 1.1 Cavity transmission for resonant and integrated CEAS, as well as direct absorption over the effective pathlength $L_{\text{eff}} = (2\mathcal{F}/\pi)L_{\text{c}} = 10$ km, all as functions of the absorption coefficient α. The CEAS signals are normalized to the respective zero absorption values

of time running average, which corresponds to an integration over a spectral region much broader than cavity resonances. Such "low pass" signal filtering also becomes necessary when using lasers having a non negligible linewidth, producing a transient noisy peak profile at cavity output (more of this in Sect. 1.4.1). In the end, as the cavity output signal is smoothed or averaged over a time window, which corresponds to a tuned frequency range wider than the cavity resonance, we are really in a situation with $\beta = 1$. As before, it is difficult to understand this by considering the signals in the time domain, since we have to convolute the time-domain cavity response function (the linear response Green's function) with the frequency swept source field (including noise), then integrate the result in time. As before, we can find a simpler description in the frequency domain, which will yield the same conclusions as in the time domain, but more easily and directly. We will use again the fact that the average cavity output spectrum is the product of the averaged source spectrum times the cavity transmission spectrum. The source spectrum to be considered is the FT of the laser field over an observation time window that includes the passage through resonance. A monochromatic sine wave frequency-swept at a constant rate over a spectral interval can be readily shown (e.g. by numerical FT) to have a flat power spectral density distribution over that interval, independently of the sweep rate. This clearly shows that swept-CEAS with integrated cavity output is indeed equivalent to BB-CEAS in terms of enhancement factor.

We conclude this section by an interesting observation concerning the attenuation of transmitted intensity by a cavity compared with direct absorption through an hypothetic cell with the same effective absorption length, given by the Lambert-Beer law $T_{\text{LB}} = \exp(-\alpha L_{\text{eff}})$. In order to make this comparison independent of the cavity transmission level, which is usually lower than unity, we consider the cavity transmission relative to its value at zero absorption $\alpha = 0$. We consider the two extreme cases of resonant CEAS, ruled by Eq. (1.8), and BB-CEAS, ruled by Eq. (1.19). For the typical parameters used above, in particular $L_{\text{eff}} \simeq 10$ km for the resonant CEAS, we obtain the curves of Fig. 1.1 which show that BB-CEAS has the smallest

loss of signal, thus potentially the largest dynamic range, while resonant CEAS falls below it and direct absorption displays the worst case behavior by far. In practice, one should also consider that the situation is reversed when considering the available signal level: Direct absorption may in principle benefit of the full source light intensity in the limit of small sample absorption, resonant CEAS usually induces some source intensity loss, while we saw that BB-CEAS is characterized by low cavity throughput.

1.2.2 The Real World of Transverse Modes

Until now the concept of longitudinal cavity mode has been developed in a frame equivalent to a basic plane wave model, and the resonances have been found to correspond to a round trip self-reproducing condition (2π phase change). Considering the finite size of the mirrors and their curvature, the modes of a real cavity can certainly not be described by plane waves. An ensemble of functions which can be made to satisfy the round trip self-reproducing condition (by a choice of parameters) are obtained by solving Maxwell's equation for the propagation of the electromagnetic field under the paraxial approximation (small angles and small deviations of the field relative to the resonator optical axis), and by making them satisfy the cavity boundary conditions. These functions are written as the products of Hermite polynomials and a Gaussian distribution function [7, 162].

In Fig. 1.2 the profiles of several Transverse Electro-Magnetic modes are represented. The lowest-order, or fundamental mode, has a pure Gaussian-shaped transverse profile:

$$TEM_{0,0}(x, y, z, t) \propto \exp\left(-\frac{r^2}{w^2(z)} - \frac{ikr^2}{2R_{\mathrm{f}}(z)} - ikz + i\omega t + i\eta(z)\right), \qquad (1.23)$$

where for clarity we have written r^2 in place of $x^2 + y^2$, and $k = n_{\mathrm{r}}\omega/c$ where n_{r} is the refraction index and ω the optical angular frequency. We see that along the propagation axis z we have a plane wave $\exp(-ikz + i\omega t)$ (with a slowly changing phase $\eta(z)$), but this is multiplied by a Gaussian profile with radius ($1/e$ half-width) given by the function $w(z) = w_0\sqrt{1 + z^2/z_0^2}$ which has waist size w_0 at $z = 0$, and diverges appreciably over the Rayleigh length $z_0 = \pi n_{\mathrm{r}} w_0^2/\lambda$. At large distances along the propagation axis $z \gg z_0$, the beam radius increases as $w_0 z/z_0$, thus with a divergence angle $\theta \simeq \lambda/(n_{\mathrm{r}}\pi w_0)$. We see that the divergence of the Gaussian beam is inversely proportional to its waist size. This relation of the divergence to the spot size corresponds to an uncertainty principle (position vs kinetic momentum, akin Heisenberg principle in quantum mechanics), and it should be noted that Gaussian beams possess the smallest uncertainty product and thus are said to be "diffraction limited" [159]. The other Gaussian beam parameters have similar slow dependence on z. They are the wavefront curvature $R_{\mathrm{f}}(z) = z + z_0^2/z$ and the Gouy phase $\eta(z) = \arctan(z/z_0)$ (which is not zero even on the optical axis and differen-

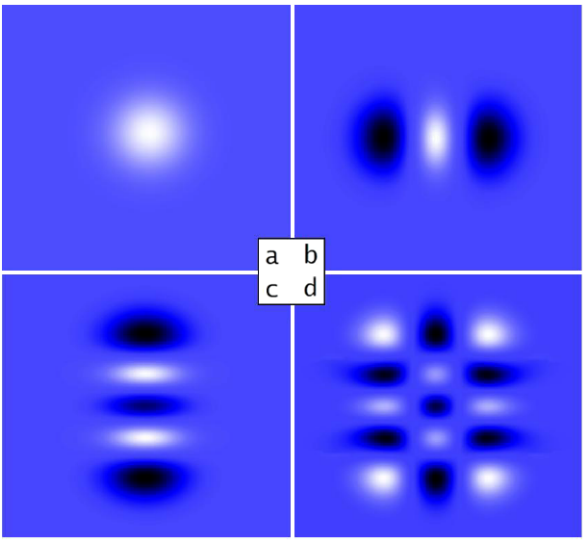

Fig. 1.2 Examples of $TEM_{m,n}$ transverse mode field distributions: (**a**) $TEM_{0,0}$, (**b**) $TEM_{2,0}$, (**c**) $TEM_{0,4}$, (**d**) $TEM_{2,4}$. The quantum numbers m and n correspond to the number of field nodes in the horizontal and vertical direction, respectively

tiates the Gaussian wave from a plane wave). The higher order *TEM* modes have the same general dependence (thus, the same beam radius and wavefront curvature as a function of z) except for an additional factor $H_m(x/w_0)H_n(y/w_0)$ where the Hermite polynomials introduce the transverse node structure (H_m possesses m zeroes), plus a Gouy phase equal to $(1+m+n)\,\eta(z)$. We see that this last modification implies a shift in the wavefronts that depends on the transverse order $m+n$.

"Mode-matching" a Gaussian shaped laser beam to a cavity consists in matching the waist size and position of the laser beam to the waist size and position of the cavity $TEM_{0,0}$ mode (and, obviously the beam should be aligned on the cavity axis). If the laser beam is not Gaussian, spatial filtering (see Sect. 1.4.2) may be used with some power loss to render it sufficiently close to Gaussian. In several implementations of CEAS, a good mode matching is needed, since excitation of higher transverse modes represent a source of noise or artifacts. Some implementations, however, such as off-axis CEAS (see Sects. 1.4.1 and 1.4.2), do exploit multi-transverse-mode excitation.

The cavity boundary conditions impose first of all that the wavefront matches the mirror surfaces, thus the z_0 parameter and the $z=0$, waist position are fixed by the cavity geometry. For the symmetric cavity that we considered until now, $z=0$ is clearly at the cavity center, and the mirror curvature R and cavity length L_c impose that $z_0=\sqrt{(2R-L_c)L_c}/2$. The resonance condition is found (as before) when the round trip phase change is a multiple of 2π, but now the whole on-axis phase term $kz+(m+n+1)\eta(z)$ is to be considered in place of kz alone. The resonant angular frequencies of the $TEM_{m,n}$ transverse modes can thus be expressed as [159]:

$$\omega_{m,n,q}=\mathrm{FSR}\left(2\pi q+4(m+n+1)\,\mathrm{atan}\sqrt{\frac{L_c}{2R-L_c}}\right), \tag{1.24}$$

where q is the longitudinal mode number. For a family of longitudinal modes of a given transverse order $m + n$, the resonances constitute a frequency comb with a specific offset but whose periodicity is always given by the same cavity FSR. We may also assume that the finesse of all transverse modes is the same up to rather large transverse orders, if the reflectivity $\mathcal{R}$ is spatially uniform. For sufficiently large transverse orders, depending on mirror transverse dimensions, diffraction losses at the mirror edges will induce a degradation of the finesse.

From Eq. (1.24) it is clear that all frequency combs with the same transverse order coincide. This is a consequence of considering a cavity with cylindrical symmetry. An interesting situation arises when the transverse spacing to the longitudinal spacing is rational: $2\,\mathrm{atan}\sqrt{L_c/(2R - L_c)} = \pi M/N$. The cavity spectrum will then consist of a series of resonances spaced by FSR/N. In practice this is obtained by adjusting the cavity length for a given set of mirrors. A simple example is the well known confocal cavity where $L_c = R$ and the transverse mode separation is exactly half the FSR ($M/N = 1/2$). The confocal cavity is also known for the fact that a beam injected off axis will follow a trajectory which closes onto itself after 2 round trips in the shape of a bow-tie, which can be understood easily by geometric ray propagation. When considering the more realistic Gaussian beam propagation, the realization of such a closed trajectory is possible via a superposition of transverse modes which are degenerate in frequency. This condition insures that the relative phases of the modes whose superposition reproduces the localized bow-tie trajectory remain constant as a function of time, so that the trajectory itself is stationary (like the modes composing it). This is related to the fact that by analogy with quantum mechanical systems, the cavity modes would also be energy eigenstates, and a stationary state must also be an energy eigenstate or a superposition of energy eigenstates with the same energy.

The general situation of an intracavity trajectory closing after N round trips has been investigated by Herriot and Kogelnik [163] and became the basis of a widespread type of multipass absorption cell. This configuration was later proposed as a basis for the off-axis CEAS scheme [65], with large cavity mirrors allowing the use of very high order transverse modes, which may be excited by an incident beam parallel but distant from the cavity axis. The interest of this configuration is that for a well chosen cavity length the cavity mode spacing may be divided by a large N since the large mirror size supports high order Herriot trajectories. It is surprising that even though N groups of degenerate modes are excited in succession as the laser frequency tunes across one cavity FSR, the resulting folded trajectory appears to be always the same for each group (a generalized bow-tie with N branches) except for fine details relating to the phases of the field along the branches of the trajectory [164]. Going back to the confocal case it is easy to understand how the bow-tie trajectory composed of the even modes which are degenerate with the 00 mode (02, 11, 20, 04, 13, 22, ..., $m + n =$ even) differs from the bow tie formed using $m + n =$ odd modes (obtained for a comb of frequencies shifted by $\mathrm{FSR}/2$): The first will be an even function for an inversion with respect to the cavity axis, while the second will be an odd function.

Going back to off-axis CEAS, from the literature it turns out that a preferred configuration is a cavity with astigmatic mirrors with no cylindrical symmetry and

which does not admit Herriot-like trajectories but rather a generalization thereof, i.e. closed trajectories whose points of reflection on the mirrors lie on a Lissajous curve. In this case, cavity modes with the same $m + n$ are split into several smaller degenerate subgroups, each describing always the same Lissajous trajectory [165], as before with differences in field phase distributions. At this stage it is preferable to postpone this discussion and conclude on off-axis CEAS at the end of Sect. 1.4.1.

1.3 Detection Limit, Noise, Fringes, and More

In absorption spectroscopy the measured transmission of a cell or an optical cavity can be related directly to the absorption per unit length of the sample, or absorption coefficient α, whose dependence on frequency gives the absorption spectrum. The well-known Lambert Beer law applies to direct absorption through a (multipass) cell, while more complex relations (see Sect. 1.2.1) exist for the case of a sample inside an optical cavity. The absorption coefficient is in turn given by the number of absorbers per unit volume times the absorption cross section, which is composed of the sum of absorption lines from all transitions between a lower to an upper quantized energy level of the absorbing molecule(s) in the sample. Each absorption line has a spectral profile with a shape (and a width) which depends on physical processes like Doppler frequency shifts from disordered molecular motion or time limitation of the transitions by perturbing binary collisions, which depend on the pressure and temperature of the sample. Using CEAS allows either measuring weak molecular transitions when using samples of known (high) concentration, or analyzing (unknown) samples for quantification of weak concentrations of one or more species.

The concentration detection limit of a given CEAS technique is then dependent on the molecular transition being probed, and it will be maximized either by using strong fundamental vibrational transitions in the mid infrared, or even stronger electronic transitions in the visible or near UV. In order to compare different techniques in a way that does not depend on the choice of spectral region (which depends on the application of interest and on the availability of laser sources), it is better to consider the detection limit in terms of the absorption coefficient, that is, the smallest detectable variation of α. To define this, it is customary to consider the rms (root mean square) noise level on the acquired spectra in the absence of molecular absorption or in the limit of very small absorption, i.e. the noise-equivalent absorption coefficient. This can be obtained by fitting a spectrum baseline section with a straight line and taking the rms of the residuals. In case the baseline is not flat because some residual molecular absorption is present, a fit of the structured absorption can also be used. An alternative that does not depend on L_c, is to indicate the smallest fractional intensity change detectable, or minimum detectable absorption, which is equal to the noise equivalent absorption times the sample physical length L_c.

This rms noise equivalent detection limit can present a white noise character, or it can contain oscillations produced by optical interference fringes. These are most

often the real limitation to the smallest detectable absorption. If light from the laser beam is scattered or partially reflected by an optical surface then further scattered by other surfaces in the setup to reach the detector, it will interfere with the main signal beam, and produce an oscillation when the source frequency is tuned, with period inversely proportional to the difference in pathlength between the signal and the parasite. What should be realized is that the amplitude of an optical fringe is given be the product of the fields, thus a weak parasite may be strongly amplified by beating with a strong signal, which is the base of heterodyne detection (this comes directly from the detected intensity being the squared modulus of the field). Typical fringes may be in the range of 10^{-5} of the signal, and are thus caused by a parasite having a power level of only 10^{-10} relative to the main signal. To reduce fringes by a factor 10 it is necessary to reduce parasites reaching the detector by a factor 100, which gives a feeling for the difficulty in eliminating this effect.

An illustrative case is the NICE-OHMS technique, which achieved a performance limited by the shot noise level on the detected light signal, giving a rms noise on a measured spectrum corresponding to 10^{-14}/cm absorption with 1 s averaging [83]. That was however the noise level observed over a tiny tuning range, a few MHz being enough to obtain the sub-Doppler saturation Lamb dip of a molecular transition, which was the scope of the demonstration. In contrast, NICE-OHMS applications to Doppler broadened molecular spectra could not get really close to that performance [88]. Indeed the typical period of interference fringes depends on the size of the experimental settings, thus typically these are on the order of 1/1 m, or 0.01 cm^{-1}. This is just below the Doppler width but largely above the width of saturation dips, which explains why fringes where not such a nuisance in the first experiment.

When comparing different techniques it is therefore important to be careful. Notably, it is necessary to consider the noise level that is finally obtained on the baseline of an acquired spectrum for a given measurement time, independently of intermediate performance indicators. In this respect, the detection limit is usually reported in terms of the noise equivalent absorption for 1 Hz bandpass, i.e. for 1 s averaging per data point (or better per spectral element, another relevant concept discussed below). However, some techniques are able to provide N spectral data points in 1 s by parallel detection or just a fast frequency tuning. In this case, it is also usual to normalize the detection limit by $\sqrt{N}$, since the acquisition of N spectrally distinct points could be considered as equivalent to N independent values to be averaged for a single spectral element. This equivalence holds only in the limit of data affected by white noise, but not in the presence of fringes or other noise sources, usually having a stronger contribution at longer timescales ("$1/f$" type of noise, associated to setup drifts).

A couple of examples will clarify this point. An acquisition of 100 spectral datapoints in 1 s may yield a spectrum with a relatively large noise level σ_α where fringes are not visible. Averaging this spectrum 100 times would decrease the white noise component by a factor 10 and could reveal the fringes, which normally are stationary over relatively long time scales. These fringes would then dominate the noise level of the spectrum, ending up with a total noise level larger than $\sigma_\alpha/\sqrt{N}$. Thus, while it is reasonable to take into account the number of datapoints provided by a

setup by consolidating it with the detection limit, the resulting value $\sigma_\alpha/\sqrt{N}$ should not be considered as a true detection limit, but rather as a "figure of merit", useful for comparing with other setups. A similar situation occurs even in the absence of fringes, when averaging a signal does not improve its fluctuations as $1/\sqrt{N}$, due to changing parameters (optical alignment, but also sample pressure and temperature, and more). In that case, spectral baseline drift in shape or level may occur without having any visible fringes.

In ring-down measurements it is often remarked that the signal quality of a single event allows an exponential fit of good quality (with flat residuals displaying uniform noise level). This yields a ring-down time estimate τ with a statistical error bar provided by the (nonlinear) fit starting from the signal noise level (the rms of the fit residuals, in practice). That single-shot noise level σ_τ is correctly estimated if the time data points are uncorrelated [145], which is not the case, for instance, if the analog to digital conversion rate is faster than the photodetector amplifier bandpass (the reverse situation is also not desirable since the undersampled signal will appear more noisy than it is). The single-shot noise is usually found to be smaller than the shot to shot fluctuations, the rms noise from an ensemble of ring-down measurements. It may be useful to provide here a relation for estimating the shot noise level for a single ring-down signal which is obtained in the case of nonlinear fitting with the proper weighting (Eq. (17) in [23], see also [145]):

$$\frac{\sigma_\tau^{\mathrm{SN}}}{\tau} = \frac{1}{\sqrt{I_0 \tau}}, \tag{1.25}$$

where $I_0 = \eta P/e$ is the flux of photoelectrons generated in the detector at the beginning of the digitized ring-down signal, dependent on the optical power P [W] (at the beginning of ring-down), the detector sensitivity η [A/W], and the electron charge e [C].

To complicate things, such an ensemble of measurements can be obtained by scanning the laser over a baseline section or just by keeping the laser frequency fixed on a single spectral element. In the first case the effect of fringes may become visible as they give a clear pattern on the data, and the rms of this ensemble would allow a realistic estimate of the total noise affecting the spectral profiles which are delivered by the setup. The second case, if the ensemble is obtained in a short time, delivers rms fluctuations closer to the ideal single-shot value, if no other noise sources affect the signal besides fringes. This is certainly an important test, but clearly does not give a fair assessment of global system performance.

The Allan variance (AV) concept originally developed to characterize the performance of clock in terms of frequency stability [166], has been applied to characterize the performance of absorption spectroscopy [59, 167, 168] but it has the disadvantage of being a one-variable evaluation test, which can be directly applied to a single spectral point at a time, but not to a complete spectral section. It delivers information about the time variability of fringes or of other baseline drift mechanisms, which affect the single spectral point. However, as above for the rms fluctuations of an ensemble of measurements at the same spectral point, the AV of a spectral

point is not representative of the spectral noise level delivered by a setup if this includes fringes or other frequency-dependent artifacts. Indeed on sufficiently short time scales a fringe does not move and does not produce an effect at the single point level, while it certainly affects a spectral profile as a whole, as we discussed above. At the end, it is more appropriate to consider the rms value of a baseline section of a spectrum, or the rms of the residuals after fitting a section of a spectrum using an appropriate model of the molecular absorption being present in it [98]. This rms value, if plotted against the averaging time T, yields a curve resembling an AV plot, decreasing as $1/\sqrt{T}$ as long as white noise is dominant, but no longer decreasing as soon as fringes or other spectral artifacts produce deviations from the fit model.

An AV plot (as a function of averaging time) [167] is however useful to quantitatively estimate the precision in the determination of some spectral fit parameters, for instance line intensities that are proportional to the concentrations of the absorbing molecules: If these are kept fixed by providing a stationary sample, the Allan variance will tell over what time interval the sample concentration can be averaged before drifts become dominant, and the AV value for a given averaging time will provide a true estimate of the rms fluctuations of concentration averaged over this time interval. Also, the time after which the AV starts increasing will indicate the stability time of the setup. Calibration procedures will allow to obtain the measurements of highest accuracy if they are realized within this time frame. For example, an unknown sample measurement and a calibrated sample measurement (of the same duration) should fit inside this stability interval in order that the second can be really useful to calibrate the value of the first within an error given by the minimum of the AV [168]. Making a calibration over a longer time span would allow for large instrumental drifts and reduce the effectiveness of the calibration, the AV corresponding to the longer interval will still give an estimate of the (larger) calibration error.

Spectral resolution and "spectral element" are other concepts that play an important role in spectroscopy or even in trace analysis, as long as this depends on fitting of spectral profiles. A spectral element does not necessarily coincide with a single datapoint in an acquired spectrum, as sometimes is assumed. This will be the case only if datapoint separation is larger than the spectral resolution. This is usually represented by an apparatus spectral response function, which may for example correspond to a laser line width, or to a spectrograph resolution in case of a broad band source. More simply one just considers the FWHM of the apparatus function as being the spectral resolution, even though it is clear that its shape is also relevant. A spectrum where datapoints are closer than this FWHM will be oversampled and close-by datapoints will be correlated. This is analogous to sampling a time signal at time intervals shorter than the time response of the signal chain generating it. In some cases datapoints may be at a separation larger than the spectral width that they correspond to. This is the case of CEAS schemes where measurements are obtained only for the $TEM_{0,0}$ cavity modes (and these are spectrally stable in time), where the spectral resolution may be considered as corresponding to the mode width, while their separation is $\mathcal{F}$ times larger. Another example is a 1 MHz linewidth laser which is tuned in jumps of 100 MHz to obtain an absorption spectrum.

1.4 Coupling of Light into a High Finesse Optical Cavity

We will now begin the description of different schemes for coupling light from various sources, not only lasers, into a high finesse cavity. All these schemes have to take into account, more or less explicitly, the resonant properties of optical cavities that we have introduced above. The logical order we have chosen follows loosely the historical developments outlined earlier.

1.4.1 Single Mode Injection: From the Ideal Monochromatic Laser to the Realistic Noisy Laser

In Sect. 1.2.1 we considered the properties of optical cavities, avoiding as much as possible any reference to a specific light source. Here we consider how cavity response combines in the spectral or time domain with different types of light sources.

Some of the most refined CEAS schemes are based on frequency locking of a CW narrow-line laser to a cavity, and are well described by the monochromatic stationary excitation model considered in Sect. 1.2.1, especially if the locking bandwidth is sufficient to squeeze the laser spectrum inside the cavity resonance linewidth. These schemes deliver a precise frequency axis, optimized cavity transmission, and usually high acquisition rates, at the price of increased experimental complexity [38, 55, 83, 169].

Several methods exist for locking a "single frequency" laser to an optical cavity, and the performance of the locking (such as the fact that the laser linewidth is reduced with respect to that of the free running laser), is generally increases with the bandwidth of the lock loop. This is a combination of the bandwidth of the system used to obtain an "error signal" (a signal proportional to the frequency difference between the laser emission and the cavity resonance) and of the bandpass of the control system acting on the laser, or on the cavity resonance frequency. There are not many general reviews dealing with different techniques to generate the error signal [170–172] and efficient methods to control laser frequency or cavity resonance frequency, thus we just cite the one by Hall [173].

Simpler CEAS schemes demand that the source optical frequency is swept through the cavity resonances, thus the cavity temporal response has to be taken into account. For the time being, we will continue considering mode matched cavity injection and neglecting the evolution of the field in the transverse direction as only the fundamental $TEM_{0,0}$ cavity mode is excited.

The temporal response of a cavity mode corresponds to the process of building up the intracavity field by the input field, or else to the field decay when the input is interrupted. The cavity response time, i.e. the characteristic time of such transient effects, is the ring-down time. As we have already seen, the field amplitude inside the cavity is governed by the interference (sum) of fields injected over multiple round trips. The field transmitted by the input mirror constitutes a source term for the field circulating intracavity, while the loss term is given at least by the leakage

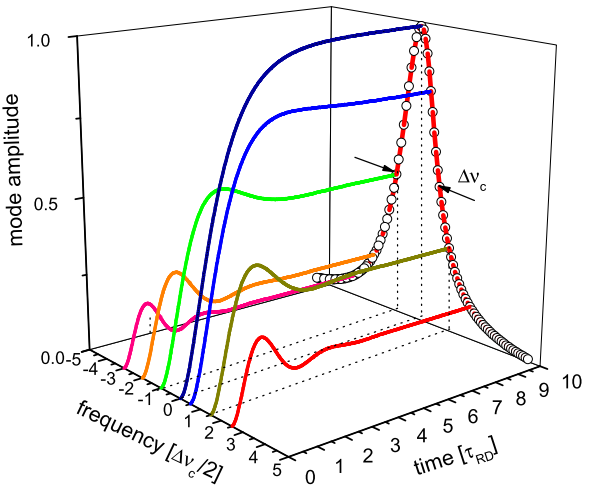

Fig. 1.3 Transient response of a cavity mode excited by a monochromatic laser wave. The ideal laser is switched on at the origin of time and the output of a lossless ideal cavity is calculated as a function of time for different mismatches between the laser frequency and the resonance. After a transient behavior, revealing damped oscillations with a period proportional to inverse of the frequencies mismatch, a stationary state corresponding to the cavity mode amplitude is attained

outside the cavity through both mirrors, if we neglect the absorption and scattering losses, or sample absorption.

At exact resonance, the input field interferes constructively with a previously injected field persisting in the cavity. Starting with an empty cavity, as the incoming field is switched on, the source term dominates over the (initially null) leaking field and the intracavity field grows. After enough round trips the buildup will be large enough to make the loss term equal to the source term. The stationary condition corresponding to maximum transmission of a cavity mode is then obtained.

For an optical frequency slightly detuned above or below the cavity resonance, the input field transmitted by the entrance mirror has a small phase difference with the field injected one round trip earlier. This shift cumulates with the number of considered round trips. If there were no field attenuation, fields consecutively injected over few round trips would interfere constructively while interference would become destructive with fields in the past whose cumulated phase shift is close to π. For longer times, constructive interferences would reappear, and so forth. But due to losses the intracavity field still reaches a stationary state given the exponentially smaller amplitudes of field components injected further in the past. As long as the phase shift is small compared to π the field buildup is still relevant. For larger detuning the oscillation becomes faster and the steady state is established at a lower buildup level. This behavior is illustrated by simulations in Fig. 1.3. For higher reflectivity mirrors, the reduced field damping makes interference effects last longer with tolerance for a smaller mismatch between an optical frequency and the exact resonance resulting in a reduced cavity mode linewidth.

These oscillations before reaching the steady state admit a perhaps surprising physical interpretation. They can be considered as a beating note of the incoming field frequency with the cavity resonance frequency. When the field is switched

on abruptly, its frequency is not at once well defined, therefore initially the cavity begins to be excited even at resonance. Before the field frequency becomes defined better with respect to its separation from the cavity resonance, a time equal to the reciprocal of the frequency difference must elapse, and up to this time the field builds up also at resonance. At that point a beating starts appearing between a transient excitation of the resonance, which dies off exponentially, and the buildup at the incoming frequency which continues up to steady state. The same kind of argument allows to understand that the cavity will produce a ring-down decay signal centered at the resonance frequency even though the excitation occurs off resonance [17]. As it can be confirmed by a rigorous calculation based on Laplace transform theory, a condition to observe a free ring-down decay is that the interruption of the incoming field is faster than the ring-down time itself [17]. Then, the cavity response time dominates the field extinction time and also determines the resolution to which the spectrum of the decaying field can be defined, given by the inverse of this time and coinciding with the cavity resonance profile.

We can now consider several input waves of equal intensity and with frequencies uniformly distributed around the resonance, which are switched on together and produce each a buildup as in Fig. 1.3. This corresponds to the case of a spectrally broad source with respect to the cavity resonance. During the first round trip, all input waves are multiplied by $\mathbf{t}$ and the intracavity field is weak but uniform: No interference effect has yet occurred. As time passes, interference occurs over more and more round trips. The intracavity spectral components closer to resonance continue to build up for longer times, while the further away the earlier the buildup terminates (with oscillations around a lower and lower asymptotic field level). As a result, interference makes the intracavity field to develop a spectrum narrower and narrower in time until full buildup and a stationary state is attained. In this "spectral evolution" it can be shown that the product of an intracavity field linewidth and the corresponding buildup time (the time from the beginning of the broad band injection, during which the cavity analyzes the input field) conforms to the FT limit ($\geq 1/\pi$).

This picture can however be misleading. It should be realized that the spectral envelope one can deduce from Fig. 1.3 for a given buildup time cannot be defined over time intervals shorter than that very buildup time. Due to the uncertainty relation there is no such thing as an "instantaneous" intracavity spectral envelope. If one tries to analyze the spectral envelope of the cavity output field at a buildup time t_b, one will need an observation time of at least t_b before being able to attain a spectral resolution sufficient to resolve that profile.[7]

Considerations of this type allow an intuitive physical understanding of cavity excitation as well as the realization that even under pulsed excitation, with a broad

[7] Any spectrograph will present an effective observation time inversely proportional to its resolution. An interesting case is the grating spectrograph, where the measurement time corresponds to the difference in delay of light paths reaching the observation plane after being diffracted at the opposite edges of the grating.

input spectrum and a short excitation time, the intracavity field (and cavity transmission) has a spectrum composed by narrow resonances whose width can be defined only over the long cavity response time. As an illustration, consider a pulse injected in the cavity and shorter than its round-trip time. The cavity output will appear composed of replicas of this pulse spaced by the round trip time ($2L_c$ divided by the group velocity, which is the propagation speed of the pulse inside the cavity, accounting for dispersion effects). The whole train of decaying pulses will present a comb-like spectrum made of the excited cavity resonances lying under the initial pulse spectral envelope. But if one analyzes each replica individually (by using a fast optical switch), only the envelope will be there, and no cavity modes. Likewise, molecules inside the cavity need to see the whole time series of ringing-down pulses in order to produce an observable response which takes into account the interference effects which create the cavity resonances and the almost null average field value in the frequency intervals between them. As we will see later for the case of frequency combs, the periodicity in frequency of the cavity resonances is not accidental but corresponds by FT to the time periodicity of the pulse train. We can also understand now that the cavity mode spacing in the presence of intracavity dispersion is given by the inverse of the cavity round-trip time calculated using the group velocity.[8]

It is now time to consider a monochromatic laser wave continuously tuned across a fixed cavity resonance, as required by several CEAS techniques. We would expect to recover the spectral cavity mode profile after converting the tuning time to frequency by using the scanning speed W in units Hz/s. However for this to be true, W should be slow enough that for each frequency there is time to achieve the stationary regime of the intracavity field. This adiabatic regime is realized when the duration of the passage through the resonance (width $\Delta\nu_c$) is much longer than τ_{RD}, the cavity response time: $W \ll \Delta\nu_c/\tau_{RD}$. Above this tuning speed as the input frequency approaches the resonance the field starts building up, but without attaining the steady state it starts decreasing by destructive interference after the tuning frequency has gone across the resonance. At the same time a beating appears between the input field and the field partially built-up at the resonance, which exponentially decays. In addition, the phase shift considered above between successively injected fields is now increasing in time quadratically as the frequency mismatch increases linearly, thus the beating has blue-chirped oscillations (see Fig. 1.4). This ringing effect is readily observable with a narrow line laser and moderate cavity finesse [174] and has been the subject of several studies [175–178]. Finally, in the limit of large W the regime of impulsive excitation is attained, with a short buildup time resulting in a small output amplitude, and a time response approaching a single exponential decay with superimposed fast and negligibly small oscillations. This excitation regime has enabled fast CRDS measurement with CW lasers using a simplified experimental setup [50, 51, 53, 179–181], notably avoiding the need for a fast optical switch.

The widespread CW-CRDS scheme exploits the larger cavity buildup generally obtained with a smaller tuning speed and requires a fast optical switch (typically an

[8] See also footnotes 4 and 5.

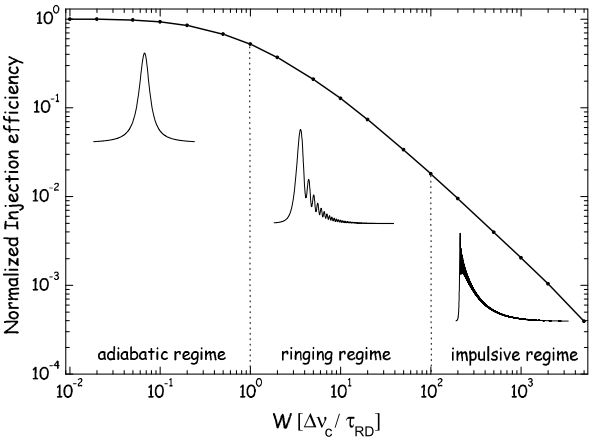

Fig. 1.4 Injection efficiency of a lossless cavity as a function of the relative laser-cavity frequency scanning speed W expressed in natural cavity units $\Delta\nu_c/\tau_{RD}$. Different sections of this curve are associated with a specific injection regime and transmission profile

acoustooptic deflector, but see [44]) placed at the cavity input to interrupt the injection when sufficient signal is detected at cavity output during a passage through resonance. In practice, rather than tuning the laser and obtain one resonance per cavity FSR, it is usually more convenient to modulate the cavity mode position across the fixed laser frequency. This is obtained by placing one of the cavity mirrors on a piezoelectric mount to modulate the cavity length. This also enables a finer tuning if the laser frequency can be continuously adjusted. However spectral resolution is no more limited by the cavity mode width (and jitter from vibrations and drift) but by the laser linewidth and jitter, and additionally by the scanning cavity mode frequency. Concerning the temporal profile at cavity output during a passage through resonance, it can be shown that this situation is strictly equivalent to the previous one. The pertinent parameter is the relative laser-cavity frequency change. This equivalence [178] rests on the correspondence $v/L_c = W/\nu$ where v is the mirror speed and ν is the optical frequency at resonance. The growing phase shift now originates from the Doppler shift of the wave at each reflection off the moving mirror. The only difference lies in the spectral analysis of a ring-down event obtained after switching off the laser beam. In case of a laser frequency sweep, the optical frequency of the ring-down signal is determined by the frequency of the resonance, which is stationary even if it may drift over time scales usually longer than the ring-down event. In case of a cavity length sweep, the frequency of the ring-down signal is determined by a resonance frequency which matches the laser frequency when injection occurs, but which continues its scan after laser interruption and over the duration of the ring-down. For a typical finesse used in CRDS and scanning speeds satisfying a compromise between signal level and acquisition rate, one estimates a frequency shift of several % of the cavity FSR during the ring-down. Such a limitation to the spectral resolution, however, can be mitigated using a tracking system that modulates the cavity resonance over a small range around the laser frequency. This also allows increasing the frequency of passages through resonance using a

lower frequency scanning speed, while reducing spurious injection events due to transverse modes (which would produce different ring-down times).

Previous discussions, and in particular the observation of the ringing effect, are based on the explicit assumption of a perfect monochromatic source. In practice this situation is approached if the laser coherence time τ_L is longer than the time of passage through the cavity resonance, which in addition should be shorter than the cavity response time. In the frequency domain, this corresponds to a laser linewidth $\Delta\nu_{\text{las}}$ narrow compared to the inverse of the time of passage. Unfortunately, especially when considering tunable semiconductor lasers, the situation is reversed: DFB diode lasers and ECDLs have short term linewidths (μs to ms timescales) in the MHz or 0.1 MHz range, respectively, while CRDS often features ring-down times in excess of 10 μs, corresponding to mode linewidths of a few tens of kHz, and below.

The spectral line profile of a CW laser is not a simple concept. It could be considered as a description of the fluctuations of the laser frequency, a sort of distribution of the instantaneous laser frequency values weighted by their temporal occurrence. It reflects the fluctuations of physical parameters determining the laser frequency, such as the laser cavity length, the laser pumping process (the injection current for a diode laser), the dye jet thickness for a dye laser, *etc*. Besides technical fluctuations, the very process of laser emission produces the fundamental Schawlow-Townes linewidth [182], due to spontaneous emission by the laser gain: Spontaneous photons with a random phase add over time to the coherent photon flux circulating inside the laser cavity and produce small phase jumps (random in time and magnitude), and therewith an average diffusion of the phase of the laser field. In this limit it can be shown that the laser lineshape is a Lorentzian of width $\Delta\nu_{\text{las}}$ proportional to the ratio of the spontaneous emission rate over the intracavity laser photon flux. The inverse of this is the laser coherence time τ_L corresponding to the time needed in average for a phase diffusion of one radian. The presence of technical noise changes the laser line profile and renders it time dependent, in particular with a distribution of emitted frequencies becoming broader over longer observation times.

In order to get a sound picture of what the laser spectral profile represents and how it relates to the phase noise and its spectral distribution, it would be necessary to refer to the exact definition of power spectral density of a field as the FT of its time autocorrelation function, which is not an easy subject. However, it was recently remarked that this admits a simplified understanding, with a computational scheme allowing to easily go from the phase/frequency noise spectrum to the emission linewidth [183], whose validity was confirmed experimentally [184].

Here, it will be sufficient to retain that a CW laser can be described realistically as a "locally monochromatic" carrier wave affected by a random-walk of the phase (a diffusion process resulting in an average phase drift proportional to $\sqrt{t}$) induced by spontaneous emission, plus a (smoother) technical drift of the carrier frequency itself (e.g. as the laser cavity drifts). This frequency change integrated over time also results in a phase drift, but linear or even quadratic in time. The characteristic time

over which phase drift remains small (relative to 1) is defined as the laser coherence time τ_L: For longer times the accumulated phase change becomes distributed uniformly over 2π, and the autocorrelation function drops to zero.

When a CW laser is tuned across a cavity resonance, let us name τ_p the characteristic time given by the cavity linewidth divided by the relative laser-cavity tuning speed, $\tau_p = \Delta\nu_c/W$. This represents the minimum time of passage through resonance that would be realized for a monochromatic wave, while a noisy laser wave with a broader frequency distribution will usually take a longer time. Let us start with τ_p larger than the cavity response time τ_{RD}. If this is also larger than the laser coherence time τ_L, the wave admitted in the cavity will experience phase diffusion during the buildup. When this diffusion attains π the incoming wave will be interfering destructively with the field previously constructed inside the cavity, resulting in the intracavity field annihilation before starting the buildup of a new field with a new relative phase. This process has been reproduced experimentally by inducing abrupt π phase jumps in a long coherence time laser [185]. Such sudden large phase changes were actually observed to induce a cavity field decay sensibly faster than the ring-down time.

Now, a τ_L larger than τ_{RD}, but still smaller than τ_p, gives a regime where the cavity is able to attain a full buildup after which the resonance conditions continues for some time. The intracavity field will then follow adiabatically the slow laser phase/frequency drifts. In this regime the cavity output may still present amplitude fluctuations as the wave central frequency (the carrier) fluctuates relative to the cavity mode linewidth during τ_p. Also, in this regime the cavity output noise spectrum will be limited by the cavity response bandpass given by $1/2\pi\tau_{RD}$, and the output will drop to zero only when the carrier will go completely out of resonance.

On the other hand, as the laser tuning speed is increased until τ_p becomes comparable, then smaller than τ_L, the cavity output will become closer and closer to the monochromatic limit, irrespective of τ_{RD}, and eventually appear unaffected by laser phase or frequency noise [178]. The ringing effect will be observable in this case if the monochromatic limit is achieved for not too high a tuning speed. Otherwise, an impulsive excitation will be obtained with a ringing too small and too fast to be observable.

Let us now turn to the subject of cavity injection efficiency. At a first sight, cavity output intensity would appear to be determined by considering that a part of the laser spectrum has been sampled by the cavity mode, without accounting for the frequency/amplitude noise projection described above. For a laser linewidth $\Delta\nu_{las}$ larger than the cavity resonance linewidth $\Delta\nu_c$, the maximum power fraction transmitted by a cavity is then taken to be $\Delta\nu_c/\Delta\nu_{las}$. This matches observations only if the time of passage is larger than τ_{RD}, and additionally, only considering time-averaged values over an ensemble of transmission profiles in order to wash out the large amplitude fluctuations that will be observed. In fact, because of the spiky character of transmission in the presence of fast laser phase fluctuations (if τ_L is smaller than other timescales) the effective maximum cavity transmission will be several times higher than the average value set by $\Delta\nu_c/\Delta\nu_{las}$, as seen in Fig. 1.5. For frequency tuning speeds such that the time of passage drops below τ_{RD}, this behavior

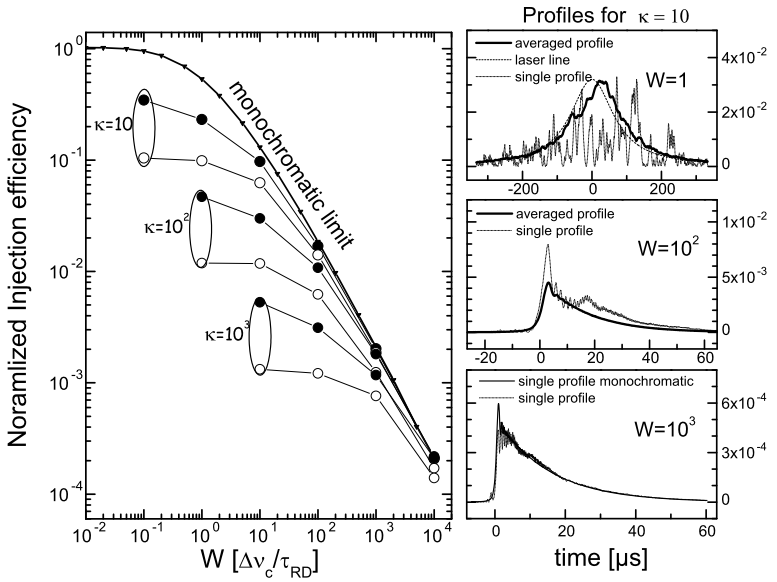

Fig. 1.5 *Left panel*: Injection efficiency for different laser linewidths. Data are extracted from simulated profiles as shown in the *right panel*. *Open circle* corresponds to maxima of averaged profiles, *full circle* corresponds to the averaged value of single profile maxima. *Right panel*: Simulated profiles obtained by a passage through resonance when the laser linewidth is ten times the cavity mode linewidth, $\kappa = \Delta\nu_{las}/\Delta\nu_c = 10$, for different values of the scanning speed (in cavity units). For $W = 1$ and 10^2 one-shot and averaged profiles (over 200 samples) are shown. For $W = 10^3$ a direct comparison of the one-shot profile with the monochromatic limit becomes possible. All simulation come from the model detailed in [178]

persists but the average transmission becomes inversely proportional to W due to a frustrated buildup, then the fluctuations disappear when the monochromatic limit is attained (for τ_L longer than the time of passage).

After these rather qualitative remarks, we conclude this section with a short review of more technical studies which have been devoted to the cavity excitation with CW lasers and especially to the modelling of the intracavity optical field. This was a general need in contexts as diverse as high resolution Fabry-Perot analyzers [174, 175] (in order to interpret asymmetric response profiles), measurement of laser cavity finesse [51, 176] (for values of $\mathcal{F}$ too high for the usual Airy-peak width measurement method and too low for easy ring-down time determination, especially with short cavities), gravitational wave detection based on optical resonators [177, 186] (as the Pound-Drever-Hall error signal used to correct resonator length variations is distorted at high correction speed), in cavity-QED [185] (in which the atom's trajectory could be better controlled by using fast changes of the photon field), and of course in the frame of CEAS developments [50, 178] to improve the understanding of laser-cavity coupling.

In these studies, three different approaches were exploited. One is based on the transfer function formalism in the time domain, where cavity output results as the

convolution of the incident field with the cavity impulsive response. Another uses the field expressed as a sum of contributions from each round trip where a fast recursive algorithm can be used to describe the field evolution. The last approach is a continuum version of the previous one, as it uses differential equations for the intracavity field evolution. All these studies agree perfectly with experience in the case of the monochromatic wave approximation, but only three of them address the question of the laser linewidth. Li and co-workers were the first to attempt taking the laser linewidth into account [175] but naively they used the inverse FT of the laser line to describe its field. This actually leads to a temporally limited optical field which is inconsistent with a CW laser. An alternative treatment was proposed by Hahn and co-worker [50] who used a weighted sum over all the monochromatic temporal profiles calculated for frequencies composing the laser lineshape. This clearly does not reproduce the cavity output fluctuations but reproduces quite correctly the coupling efficiency as a function of the scanning speed and for different laser linewidths. Finally, Morville et al. [178] developed a model with the laser linewidth as a phase diffusion process easily included in a field expression as a series as in Eq. (1.1). This enables to reproduce experimental profiles for all configurations, that is to say, for all laser linewidths and scanning speeds, as long as the correct noise model is used in the calculation. For an analytical treatment see also [43].

1.4.2 Multi-mode Injection (Longitudinal and Transverse): Incoherent Pulsed Lasers

Until now, the simple and widespread CEAS scheme also named ICOS [63, 64] where the cavity transmission is monitored (or integrated by using a slow-response photodetector) as the laser is tuned, has not been considered since it is usually implemented without mode matching, given that multi-transverse-mode excitation delivers a smoother cavity output. In that case however, one would expect to observe a periodic transmission pattern, since the same sequence of transverse modes is excited as the laser tunes over each cavity FSR: In principle these transverse modes should be excited always with the same efficiency given by the transverse superposition integral of the incoming beam with each transverse mode profile. In practice, laser phase/frequency noise may induce strong fluctuations well above this periodic structure. Such fluctuations are often reported as a problem in CEAS, and are usually attributed to cavity acoustic fluctuations, which usually play a minor role and only at timescales much longer than the typical duration of a passage through resonance. From the above discussion it is evident that in order to reduce such noise effects it should be enough to use a sufficiently fast laser scan, as illustrated by Bakowski et al. [179]. These authors obtained in CW-CRDS a detection limit close to what other groups demonstrated with similar cavity characteristics but with a much slower acquisition time. On the other hand, excessively fast frequency tuning may induce a distortion of the absorption line profiles when using CEAS, due to the limited cavity response time.

Another CEAS scheme, namely off-axis ICOS, positively exploits transverse mode excitation by off-axis alignment of the laser beam [65–67]. As mentioned earlier in Sect. 1.2.1, a cavity with large astigmatic mirrors is required, with its length adjusted in order to obtain specific trajectories whose impact points on the mirrors form a Lissajous-like figure, rather than just a circle or an ellipse as in the basic Herriot cell. Here we can add to that understanding the fact that a given laser injected into such a cavity is characterized by a finite linewidth and an associated coherence length, as we learned from the previous section. The laser beam launched into an intracavity trajectory folding onto itself after N round trips, with N possibly as large as 100, will have lost its coherence and will possess a random phase with respect to new incoming radiation, resulting in zero average interference. This means that as the laser frequency is tuned the cavity transmission will basically present no resonances. An equivalent point of view is that the cavity FSR is divided by N equally spaced groups of degenerate resonances, and FSR/N may be smaller than the laser linewidth so that the cavity mode structure appears to the laser like an effective continuum transmission. However in practice this would demand very large mirrors and an excessive precision in their surface quality and the adjustment of their distance to satisfy the reentrant condition well enough, especially in the limit of high finesse. Using an astigmatic cavity configuration allows for larger N with still reasonably small mirrors, since the N distinct impact spots are now distributed over a Lissajous folded curve with a large perimeter extending uniformly over the entire mirror surface, rather than being constrained over the shorter perimeter of a circle running close to the mirror edges. As we mentioned in Sect. 1.2.1, the exact degeneracy in N groups of modes is broken with an astigmatic cavity: But this is not a penalty because of sub-groups of still degenerate modes which are strongly clustered to form a regular structure of mode groups uniformly filling the cavity FSR period [164, 165]. In addition, the fact that as the laser scans its beam keeps describing the same folded trajectory, implies that the mirror inhomogeneity does not make a difference. Indeed the mirror spatial regions used for the multiple reflections are constant as the laser frequency scans, contrary to what happens when a non reentrant cavity configuration is used. To conclude about the off-axis ICOS technique, what we just exposed appear to be the principal reasons underlying the excellent performance demonstrated with off-axis ICOS and also justify the need for a large transverse cavity size (using mirrors of up to 5 cm diameter), which was experimentally illustrated by Engel et al. [67]. On the other hand, this large transverse cavity size is a drawback because of the large sample volume, and the need for a large detector surface for collecting the spatially extended cavity output. In the mid-IR such a detector has to be cryogenically cooled in order to obtain a reasonably low noise figure and a high bandpass.

We can now turn to another important class of developments where the laser source usually imposed multimode cavity injection, both transverse and longitudinal. Pulsed (ns) dye lasers allow very wide spectral coverage with a resolution (down to and below 0.05 cm^{-1}) sufficient to study the rotational structure of most light molecules. They are capable of fast continuous tuning by the synchronized tilt of a grating and of an etalon present in the laser cavity. By using different dyes and

nonlinear frequency doubling or tripling techniques, or Raman shifting, the whole visible range is accessible and even the near UV or the near IR are at reach. Pulsed ns Ti:Sapphire, Optical Parametric Oscillators (OPO) and other solid state laser systems extend the accessible spectral range and possess similar properties compared to dye lasers, thus should also be included in this discussion.

The high peak power available with ns lasers is often used to produce, exploit, or investigate nonlinear effects in optics or molecular spectroscopy, on the other hand these lasers suffer of a poor shot-to-shot stability not only in intensity but also in the beam profile which is far from Gaussian. In particular ns lasers cannot be used for the simplest absorption spectroscopy measurement with a sensitivity better than 10^{-3} (in terms of the detectable intensity loss). However, CRDS provides high detection sensitivity without penalty from amplitude fluctuations, at least in principle, and it fully profits of the high peak power available: As a laser pulse is transmitted through the input cavity mirror it is strongly attenuated but still enables linear absorption measurements by detecting the cavity transient response, i.e. a ring-down decay profile. The variations of the ring-down time due to sample absorption are usually detectable at the few % level even in the presence of source intensity and spatial fluctuations (and these can be strongly reduced using spatial filtering as discussed below). A 1 % variation in the ring-down of a high finesse cavity then corresponds to a very small sample absorption. Since the visible spectral range and the near UV are populated by weak vibrational overtone transitions of molecules of atmospheric or planetological interest, pulsed CRDS is a working tool highly appreciated by spectroscopists.

When considering how CRDS is implemented using a pulsed laser, we easily realize that another advantage is simplicity: It is enough to align two high reflectivity concave mirrors along the laser beam, at a separation L_c chosen well inside the stability region of the cavity [159]. Then a photodiode with high gain (typically 10^5–10^6 A/W, 1 MHz bandpass) is used to detect the cavity output signal.

We have already discussed how a cavity responds to an external excitation in the limit of a short light pulse. In the frequency domain we have to consider that the spectral width of ns lasers is typically larger than the cavity FSR (assuming $L_c \sim 1$ m) which implies that at any laser frequency at least one longitudinal cavity mode can always be excited. In particular a pulse shorter than the cavity round trip time will possess a spectrum with no structure finer than the cavity FSR. However, more rigorously we should consider the laser coherence time, which is shorter or equal to the pulse duration. Equality of pulse length and coherence time occurs for a FT-limited laser spectrum, but this is rarely realized and in general CRDS presents no real difficulty with laser pulses which are longer than the cavity round trip time [27]. Indeed, even when a pulsed laser is built to be FT limited, we still have to consider that transverse cavity modes may transmit at different frequencies. Thus in order to really observe clear effects of cavity resonances one has to use good mode matching in other to excite only the $TEM_{0,0}$ (longitudinal) cavity modes. It is then possible to observe no cavity transmission when the pulse frequency falls in between two modes [187]. A corollary of this is that if a molecular absorption line falls in between two longitudinal modes, mode matched cavity injection would make this line to be missing in the CRDS spectrum.

Pulsed CRDS easily provides measurement of the ring-down time at the 1 % level after reasonable signal averaging using relatively quick and dirty cavity injection. When using cavities of high finesse, easily exceeding 10^4 in the visible range, with ring-down times $\tau_{RD} \sim 10$ µs when using $L_c = 1$ m ($\tau_{RD} \simeq L_c/[c(1-\mathcal{R})] = \mathcal{F}/\pi \cdot L_c/c$), the detection limit should then be on the order of 3×10^{-8}/cm, in terms of the smallest detectable, or noise-equivalent, absorbance for each spectral data point. This is easily seen by considering the basic equation stating that for an absorption coefficient α by the intracavity sample the ring-down time is given by $1/\tau_{RD} = c(1-\mathcal{R})/L_c + c\alpha$, from which we deduce that the "noise equivalent" absorption is $\alpha_{ne} = (\delta\tau/\tau_{RD})/(c\tau_{RD})$.

In order to optimize the sensitivity in CRDS and go beyond such basic 'warranted' detection limit, special care must be taken with respect to mode matching, which requires spatial filtering. Without such extra efforts, pulsed CRDS is usually limited by wide fluctuations in the transverse cavity excitation patterns (fluctuation of the ensemble of excited transverse modes) obtained at each laser pulse, with non-exponential cavity output signals as a result of the beating between transverse modes and their different exponential decays. Transverse cavity modes are orthogonal so that the intensity produced by their superposition should be equal to the sum of the intensities of each mode which are all exponentially decaying after pulsed cavity excitation. However spatially non-uniform detector response (some photomultipliers are particularly bad in this respect), and mirror surface non-uniform loss or transmission, break the orthogonality and reveals the beatings [10] as it has been discussed by several authors [30–32, 42] and even exploited to monitor the transverse cavity excitation and optimize the mode matching [188–190].

Spatial filtering is a corollary of mode matching when using pulsed ns lasers. This may be obtained by using a pinhole, with typical diameter of 50 to 100 µm, through which the laser beam is focussed by choosing a lens producing a spot larger than the pinhole, so that at the focal point the beam may be considered as a plane wave which is limited by the pinhole edges and produces a diffraction Airy pattern in the far field. Focussing on the pinhole is critical: if the focal spot is too large much pulse energy will be lost, and if it is too small the beam will go through the pinhole without attenuation but without spatial filtering either. An adjustable diaphragm can be used in the far field to eliminate the rings of the Airy pattern leaving the central lobe which is close to a Gaussian profile. This cleaned quasi-Gaussian beam may then be imaged to match the cavity $TEM_{0,0}$ mode by another properly chosen lens (at appropriate distances from the pinhole and the cavity), then by looking at the cavity output spot shape and size it is possible to optimize the beam and cavity alignment. Another spatial filtering aid is using Brillouin scattering in a liquid [191], which has the advantage of eliminating the amplified spontaneous emission (ASE), spectrally broad incoherent radiation accounting for a sizable fraction of the laser power. ASE is source of artifacts in CRDS when absolute absorption measurements are desired, since it produces a multispectral ring-down component insensitive to spectrally narrow absorption lines.

1.4.3 Multi-mode Injection (Longitudinal): Coherent Pulsed Lasers, or Frequency Combs

As we mentioned in the historical outline (Sect. 1.1.1), broad-band (BB) implementations of CEAS using LEDs, lamps, or supercontinuum sources, coupled with multispectral detection at cavity output, have been successfully applied to the detection of trace species over a broad spectral range. The developments and multiple applications of BB-CEAS will be described in a dedicated chapter of this book. The principal limitation of spatially and/or spectrally incoherent sources is the inefficient cavity injection, linearly degrading with the cavity mirror transmission coefficient. The resulting power spectral density available at cavity output makes it hard to obtain very high spectral resolution over reasonable acquisition times and using reasonably high finesse cavities. Mode-Locked (ML) lasers are an expensive solution to this problem. Below we will find it convenient to first focus on the different ways of coupling a ML laser to a high finesse cavity, then to separately present different ways of measuring the spectrum transmitted by the cavity, even though the two aspects are not decoupled.

ML lasers are known to generate very short pulses, from picoseconds down to femtoseconds, with a very stable repetition rate. A few types are now available to cover the near infrared and red spectral domains directly, and nonlinear frequency conversion techniques are very efficient due to the high peak power of these sources and allow accessing a much broader spectrum. To fix ideas, we will consider a Ti:Sapphire ML laser with pulse duration $\tau = 30$ fs, a repetition rate $f_{\mathrm{rep}} = 80$ MHz, and a spectrum centered around 800 nm. The short pulse duration corresponds, if one considers the FT uncertainty principle, to a broad laser emission spectrum spanning about 30 nm (the FWHM $\Delta\nu$ is then $\sim$15 THz, with $\Delta\nu \times \tau = 0.44$ for a FT-limited Gaussian pulse), as broad as the spectrum emitted by a LED. However, again due to FT properties, it is easy to understand that the periodicity in time of laser pulses must also give a periodic signature in the frequency domain. Indeed the broad ML laser spectrum consists of a comb of narrow peaks centered at uniformly spaced frequencies, a periodic structure composed by some 180k modes in our example, whose frequency interval is equal to the laser repetition rate. The uniformity of the mode spacing of an Optical Comb (OC) may be quite remarkable, better than a few parts in 10^{17} [192, 193]. However, as mentioned in Sect. 1.1.1, the frequencies of the OC teeth are not an integer multiple of the repetition rate. This is a consequence of the difference between the phase velocity and the group velocity of the pulse propagating inside the laser cavity, which results in a relative delay between the carrier wave and the pulse envelope which accumulates from pulse to pulse. Consequently, the OC has a frequency offset f_0 as in Fig. 1.6, and the frequency of mode N is given:

$$\nu_N = f_0 + N f_{\mathrm{rep}}. \tag{1.26}$$

In a free running OC, laser phase noise results in a short term (ms) linewidth of comb modes ranging from below 100 kHz for fiber oscillators up to around

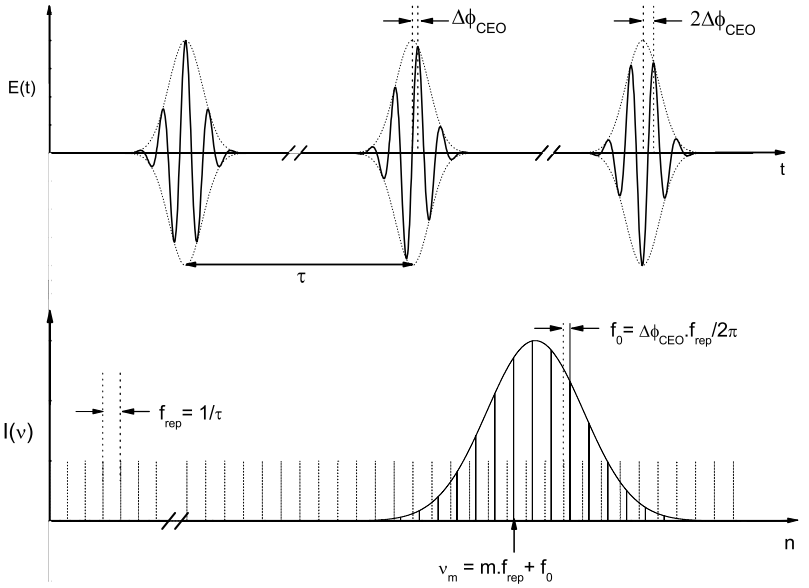

Fig. 1.6 Time-frequency correspondence of pulses delivered by a mode-locked laser (picture was inspired from Ref. [194], but not copied directly)

1 MHz for Ti:Sapphire oscillators. However, stabilization techniques have pushed the linewidth and/or the definition of modes frequencies to subhertz levels [195–197]. The consequences are remarkable in the metrology domain with respect to atomic clocks and optical frequency standards and measurements, and made the object of a Nobel prize in 2006 [198, 199].

Since an OC is clearly an easy match for a comb of cavity resonances, different comb-CEAS coupling schemes have been introduced and developed. We will generically refer to these as OC-CEAS techniques. The basic coupling scheme is obtained when the cavity FSR is exactly equal to an integer multiple of the laser repetition rate. For instance, if the high-finesse cavity length is half the laser cavity length, a choice usually leading to a reasonable cavity size, then one every two laser modes is transmitted by the cavity while the rest will be reflected (a 50 % waste of laser power). In the time domain, each laser pulse entering the cavity (by partial transmission through the input mirror) will add up to the next laser pulse after two cavity round trips, during which it will be partially transmitted by both cavity mirrors and produce two replicas at the output (of slightly decreasing amplitude). The cavity will then multiply the laser repetition rate by a factor 2. This property has been exploited to increase the laser mode spacing by a large factor [103] to allow an easier discrimination of successive frequency channels. If the cavity length is tuned across such a comb matching position, the laser spectrum envelope transmitted as a whole as an intense light burst, which can be periodically reproduced by cavity length modulation. Alternatively, the cavity length may be servo-locked to this position, which is more challenging but yields a continuous transmission with a high

signal level. The application of the simpler configuration to absorption spectroscopy was demonstrated in 2002 by Gherman et al. [105]. The second configuration had to wait 2011 to be implemented by a group well established in frequency metrology [124].

On the other hand, when the cavity length L_c is not at such an exact "global resonance" but is at δL from this point, the cavity transmitted spectrum presents a beating pattern which correspond to modes going periodically in and out of resonance [105]. A partial match of the two combs then occurs only by groups of modes spaced by the beating period $\delta\nu_b = c/2\delta L$. This "Vernier effect" can be exploited for a combined cavity injection and dispersion scheme. Gohle et al. in 2007 [112] actually succeeded resolving single comb modes by further combination of Vernier with multiplexed dispersion on a CCD array, while Thorpe et al. [113] reported low resolution Vernier CEAS spectra taken with a single element detector.

Up to this point we did not consider cavity dispersion effects nor the frequency offsets of both cavity and laser combs. Indeed, contrary to the laser OC, the free spectral range (FSR) of the cavity is not perfectly constant. The first reason is a phase shift θ at the reflection on the mirrors (the field coefficient of reflection $\mathbf{r}$ is complex and $\theta = \arg(\mathbf{r})$) and this phase shift depends on wavelength. This is due to the fact that the coating of high reflective mirrors is a stack of alternate $\lambda/4$ dielectric layers of alternate high/low refraction index which constitute a complex interferometric system with a penetration depth of the incoming field which is frequency dependent. Even though it is possible to engineer non periodic dielectric stacks to reduce this effect, this comes at the expense of the reflectivity value, the mirror losses, and also the flatness of the mirror spectral response, and a compromise has to be accepted. A second reason is that, as soon as the intracavity sample presents absorption lines, there is a dispersion associated to these because of the principle of causality (from which one derives the Kramers-Kronig relations between absorption and dispersion for a linear response system). This dispersion effect becomes particularly strong in the proximity of absorption lines, but may present a broad band dependence induced by intense absorption bands lying outside the spectral window of interest.

Both effects lead to a cavity FSR which is frequency dependent, and to an offset of the comb of cavity resonances (this is a local offset appearing when trying to approximate the resonances with a uniform comb, thus, it is also frequency dependent). To show this we consider the resonance condition for a cavity of length L_c:

$$k_m L_c - \theta = m\pi \quad \Rightarrow \quad \frac{2\pi n_r \nu_m}{c} \times L_c = m\pi + \theta \quad \Rightarrow$$

$$\nu_m = m\frac{c}{2n_r L_c} + \frac{\theta c}{2\pi n_r L_c} \quad \Rightarrow \quad \nu_m = m\mathrm{FSR}(\nu_m) + f_{0,\mathrm{cav}}(\nu_m). \quad (1.27)$$

Since FSR and $f_{0,\mathrm{cav}}$ are weakly frequently dependent through the refraction index $n_r(\nu_m)$ and $\theta(\nu_m)$, the value of ν_m is the solution of this nonlinear equation (readily obtained by numerical iteration). For normal high reflectivity mirrors and an empty cavity, one finds that change in the cavity mode spacings add up to a mismatch with

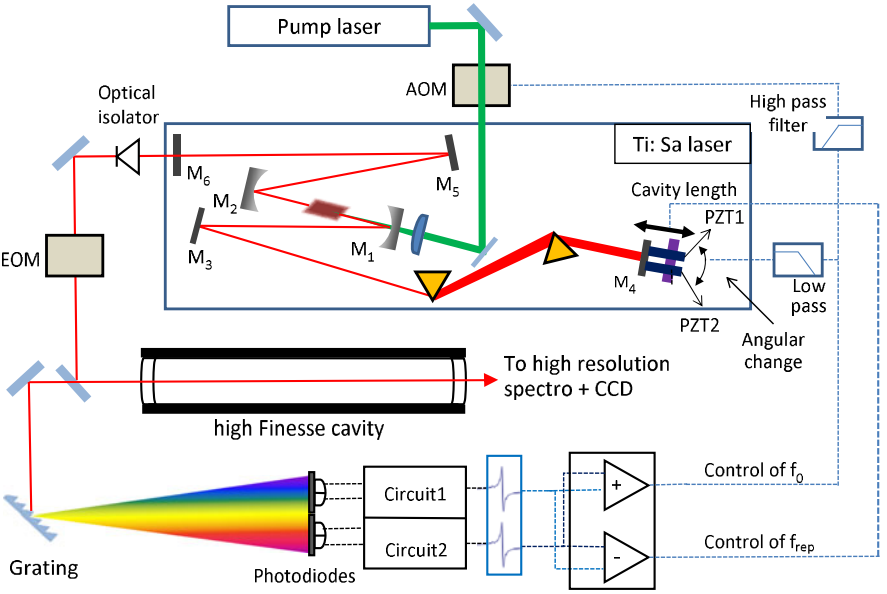

Fig. 1.7 Principle scheme of tight lock of a laser comb to a high-finesse cavity. An optical isolator protects the laser from any feedback. The electro-optic phase modulator EOM is used to obtain the locking error signal from two Pound-Drever-Hall arrangements working in parallel at different wavelengths, selected by a grating (each error signal is still produced by thousands comb teeth). f_{rep} is here controlled by a change in the cavity length by a piezoelectric transducer and f_0 is controlled at low frequency by a piezo tilt of the mirror M_4 which acts on the group velocity dispersion. This is doubled by a high frequency control of f_0 by a change of laser pump intensity using an acoustooptic modulator

the comb teeth in the MHz range for a 1 % frequency variation in the flat central region of the mirrors stopband [200]. We will see that this results in a spectral filtering effect limiting the spectral region over which an OC can be simultaneously transmitted by the cavity (in particular this occurs when using comb to cavity frequency locking) [113].

After these general remarks we would like to review in more detail the different strategies to achieve a coupling between laser and cavity combs, which may be classified as follows:

- Static continuous cavity injection by comb frequency locking;
- Transient injection at the passage through a comb quasi-resonance;
- Vernier effect in the presence of a slight combs spacing mismatch.

Maximizing cavity injection over the broadest possible spectrum requires to lock the two OC parameters, the repetition rate f_{rep} and the frequency offset f_0, for which two error signals are needed. An appealing scheme, represented in Fig. 1.7, is to duplicate and run simultaneously the same standard laser-cavity frequency locking method at two different wavelengths inside the OC spectrum [196, 201, 202]. The frequency locking method of choice is typically the Pound-Drever-Hall (PDH)

scheme [171], which can be easily coupled with a grating which spatially separates two spectral windows at the two ends of the OC spectrum. An advantage of the PDH scheme is its wide bandpass which is not limited by the cavity response time as is the case with any scheme which would exploit the cavity transmitted signal. In addition, a high S/N error signal is produced by two frequency modulation sidebands heterodyning with a strong carrier field leaking out of the cavity resonance used for the locking (once the locking kicks in).

On the other hand, a general limiting factor of frequency locking schemes is the bandpass of the servo actuators available to control the OC parameters. The use of piezoelectric actuators to adjust the laser cavity length, for example, may limit the control bandpass on f_{rep} to 10 kHz or less (see however [203]). Some fast controls do exist however (such as using an acoustooptic modulator to introduce a frequency shift equivalent to f_0) and can be used to achieve a reduction of the laser phase noise up to sufficiently high frequencies to obtain a linewidth narrowing of the comb teeth at all timescales. Indeed, a locking acting only on a low frequency region of the laser noise spectrum will allow to have zero drift of the relative comb-cavity frequency differences with very good statistics (typically resulting in an Allan variance dropping steadily with averaging time), but will not reduce the laser linewidth. The CEAS signal will then suffer from the conversion of laser phase noise to amplitude noise which we discussed in Sect. 1.4.1, even though this will be low-pass filtered by the cavity and can be efficiently removed in some detection schemes [124].

Another difficulty with tight frequency locking is associated with cavity dispersion and the frequency walk-off of the cavity modes with respect to the OC teeth. Thus, high transmission can only be maintained over a limited spectral range which tends to become narrower as the cavity finesse is increased or the locking is made tighter which is in a way equivalent to make the OC "finesse" to also increase (this may be defined as the OC f_{rep} divided by the OC modes linewidth). As we mentioned earlier, the use of mirrors with compensation of the group velocity dispersion only mitigates the problem and imposes a compromise on the attainable finesse.

In addition, at the edges of the transmitted OC spectral window, distortion of molecular absorption lines by local dispersion effects is expected and was observed [124]. Even though this can be quite well modelled, it adds complexity and uncertainty to the exploitation of the recorded spectra. This effect is easily understood by considering that at the edges of the transmitted portion of the OC spectrum, the cavity modes are systematically offset by a fraction of their linewidth then cavity transmission of the OC modes does not occur at the peak of the cavity modes. Then, a small shift of the cavity modes by the increase and decrease of the sample refraction index on opposite sides of an absorption line will result in an increase or decrease of transmission thus giving the observed asymmetric profiles [124].

Another effect which does not appear to have been considered until now, concerns the cavity enhancement factor that we discussed in Sect. 1.2.1. As we explained there, if the linewidth of the OC is comparable to that of the cavity resonances, the enhancement factor β lies in between the monochromatic case $2\mathcal{F}/\pi$ and the broad-band case $\mathcal{F}/\pi$, which poses a problem of calibration of the intensity scale of the measured molecular absorption spectra. It appears plausible that

static OC-CEAS schemes should be affected by this artifact unless a high-bandpass tight lock guarantees that the OC teeth linewidth is well below that of cavity modes (resulting in a well-defined and favorable $2\mathcal{F}/\pi$ enhancement factor).

Notwithstanding these difficulties, Foltynowicz et al. recently achieved shot-noise limited performance by using static OC-CEAS with a fast scanning FT interferometer coupled with a balanced-detector noise cancelling system, detecting 10k spectral elements in a 6 s measurement time [124], thus covering a 6 THz window around 1.55 μm with 380 MHz resolution.

The second strategy involves transient OC-CEAS coupling, or ML-CEAS as initially named [105], where ML refers to the laser source and not to the way the OC teeth are coupled to the cavity, since no actual frequency locking is involved. In ML-CEAS, the cavity length is modulated around a global comb resonance in a way that each cavity mode is rapidly swept over the corresponding OC tooth. It is also possible, and almost equivalent (see Sect. 1.4.1), to let the cavity length fixed and modulate the OC. One advantage of this scheme is that the whole laser spectrum is transmitted by the cavity with no penalty from cavity dispersion: no broadband spectral filtering, and no local spectral distortion. This also allows using standard high reflectors which may be optimized to attain the highest finesse without constraints. Even though a broad OC spectrum can be coupled through the cavity over a short time scale (down to a few μs if necessary), cavity injection results in average quite less efficient than in the locked scheme, depending on the fraction of the cavity FSR over which the comb modulation occurs. For a modulation as large as one cavity FSR, the injection efficiency is as low as for a broad-band spectrally incoherent source, but still remains the advantage of spatial coherence of an OC, which allows mode matched injection of the cavity $TEM_{0,0}$ modes. By the same token, the cavity enhancement factor is well defined but assumes the lower value of $\mathcal{F}/\pi$ valid for broad-band or swept sources (see Sect. 1.4.1) [98].

This coupling scheme is vastly simpler to implement and more robust than a tight locking technique. In particular, only one comb parameter needs to be actively driven by a fixed modulation (constant amplitude and frequency) plus a bias which is controlled in order to maintain the global resonance of the combs at the center of the modulation range.[9] The width of the modulation usually has to be increased in the presence of stronger acoustic perturbations, and the modulation frequency has to be high enough so that the passages through resonance belong to the monochromatic regime discussed in Sect. 1.4.1. We recall that in this regime all phase/frequency laser noise is not converted into amplitude noise at cavity output, contrary to what occurs at slower tuning speed.

Above, we referred to this scheme by using the term "quasi-resonance" because the active control of a single comb parameter does not allow to achieve optimal comb matching and a true simultaneous resonance of all comb teeth. The method

[9] A drift of the other comb parameter (typically f_0) will only affect the match of the combs and the width of the transmitted peak at the passage through resonance, with no impact on the measurement as long as all the comb modes go through resonance with the cavity, even if at different times.

works well even when using a secondary resonance, i.e. if the cavity comb modulation is centered around one of the peaks occurring close to the best comb match resonance (where the only residual mismatch is due to non optimal f_0 plus cavity dispersion). Indeed injection of the whole OC works well as long as the mismatch between the combs spacings is sufficiently small that there is a single beating period in frequency space between the two combs. As long as there is only one group of modes being transmitted at a time, the cavity modulation just induces a sweep of this beating across the OC spectrum. Still in other words, the final result of modulating around such a quasi-resonance is the same as using a more perfect comb match since for each modulation sweep all cavity modes will go through resonance once with their corresponding OC tooth. The only disadvantage is that a larger modulation range is required and the resulting average transmission decreases accordingly.

This ML-CEAS scheme has been implemented by sweeping the cavity length thanks to a piezoelectric transducer [105] providing 6 GHz spectral resolution over a 2 THz spectral window (330 spectral elements) in 40 ms acquisition time, using a moderate cavity finesse. It was then successfully tested for a few applications at different wavelengths with higher cavity finesse, in particular to access blue wavelengths and detect ions and radicals in a plasma discharge [106] or measure weak overtone vibrational transitions [107]. These applications fully profited of the efficient and direct frequency doubling of fs pulses.

Perhaps surprisingly, this simple scheme is capable of shot noise limited performance [98] during routine operation, with low signal levels (10 nW) available at the output of a very high finesse cavity ($\mathcal{F} = 32$k), however sufficient to fill the CCD array detector during the shortest available exposure and readout times (10 ms). This kind of detector is optimal to accumulate in parallel spectral channels the CEAS spectrum dispersed by a grating spectrograph, and is one of the key factors of this performance (given the small readout noise and high quantum efficiency). The other factor is the fast cavity modulation which eliminates spurious laser frequency/phase technical noise. The number of simultaneous spectral elements available is limited by the size of a linear CCD array detector, however two-dimensional dispersion schemes (like VIPA[10]) coupled with a CCD matrix should allow to acquire many more spectral elements with similar performance.

While the previous schemes require a resolving spectrograph at cavity output and a CCD detector, the third OC-CEAS configuration is able to economize these components by exploiting the properties of combs to achieve high spectral resolution with a number of spectral elements limited by the cavity finesse and ultimately by the number of comb teeth. A cavity displacement δL with respect to the optimal comb resonance position may be introduced on purpose, to obtain a cavity FSR slightly different of the laser repetition rate f_{rep}. A comb beating with period $\Delta\nu_b = c/2\delta L$ will be obtained in the spectral domain at cavity output, with each beat containing a group of modes in resonance with OC teeth and producing a

[10]Virtually Imaged Phased Array: Basically, a tilted glass etalon which strongly disperses the frequencies of a light beam in the plane of the tilt, usually then coupled with a grating dispersing in the orthogonal direction [204].

transmission peak in frequency. The number of modes being in resonance is smaller for faster beating and larger mismatch, but will also depend on the cavity and OC finesses. If the cavity modes are swept by acting on the cavity length, the position of the beatings will be swept and cover a complete beating period when the modes run over one cavity or laser FSR, whichever is smaller. If the comb mismatch is important, it is possible to selectively transmit a single OC tooth per beating period, but it will be necessary to introduce again a dispersive system and multiplexed (CCD) detection and combine it with the scan of the cavity length to retrieve successive absorption spectra, which will demand to be interlaced to obtain a complete mode-resolved spectrum. For instance, Gohle et al. [112] used a rotating mirror to impress successive spectra over successive lines of a CCD matrix as the cavity length was continuously tuned. The single cavity modes appeared as distinct dots on the CCD image. They demonstrated a resolution of 1 GHz over a bandwidth of 4 THz (4k spectral elements) with an acquisition time of only 10 ms. For this result they used a frequency stabilized OC which should allow in principle to achieve a frequency accuracy well below 1 GHz for each data point.

In the opposite limit of a small mismatch, only one group of modes may be transmitted at a time by the cavity as soon as $\Delta\nu_b > \Delta\nu_{\text{laser}}$ is satisfied, and spectral analysis can be obtained just using one photodiode [113]. In that case, many consecutive teeth are transmitted simultaneously by the cavity. Still Thorpe et al. reported a resolution of 5 GHz over a bandwidth of 1.6 THz (320 spectral elements) with a sweep time of 220 ms. This Vernier effect could be pushed to achieve higher resolving power over a broader laser spectrum by increasing the cavity finesse and the relative cavity-laser stability thanks to a tight locking which induces a comparable or higher OC finesse.

After considering injection schemes, we are now going to outline different detection schemes that have been coupled with OC-CEAS. For the first and second coupling schemes, cavity transmission should be analyzed with a high resolving power spectrometer. Different implementations have been tested, each presenting advantages and drawbacks. The easiest appears to be the diffractive spectrometer equipped with a linear CCD array, possessing a few thousands pixels at most. The number of spectral elements will then be limited, especially if low spectral distortion is desired, since then the spectrograph apparatus function should be wider than the pixel size. A respectable resolution for gas phase spectroscopy is then only possible over a relatively narrow spectral window [105, 110, 205].

To increase the number of spectral elements, spectral dispersion can be performed in two spatial dimensions, over a CCD matrix detector, by using a VIPA in combination with a grating [204, 206]. It is thus possible to increase the number of spectral elements and to analyze a broadband spectrum at high resolution [109]. However, using this technique beyond the near-infrared may be a challenge because of the lower sensitivity (and much higher price) of matrix detectors at longer wavelengths. Another difficulty appears to be that the VIPA is very sensitive to alignment drifts, which demands frequent acquisition of calibrations spectra [138].

An alternative to VIPA is to use a FT Spectrometer as we mentioned earlier. In that case, the detector is a simple photodiode [122, 124], but a mechanically sophisticated Michelson setup is needed to generate the interferogram. Kassi et al.

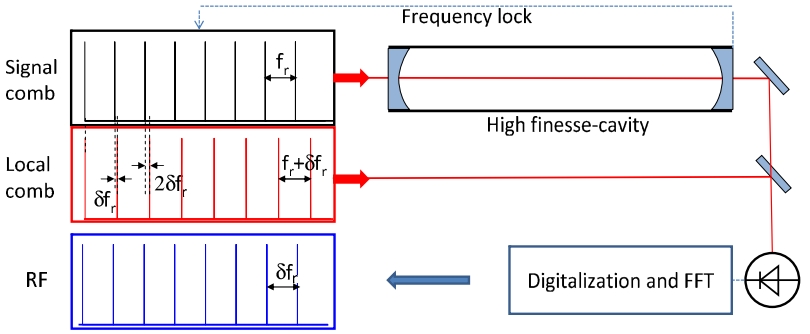

Fig. 1.8 Principle scheme of multiheterodyne detection. The absorption spectrum is shifted and compressed to the radiofrequency domain

in 2010 used commercial FT and OC systems to achieve 3 GHz resolution over 2.4 THz (800 spectral elements), with an acquisition time of minutes. A nice feature of a Michelson interferometer is that two complementary signals can be obtained whose combination eliminates common mode amplitude fluctuations. This is the feature exploited by Foltynowicz et al. [124] to obtain photon shot-noise limited FT cavity-enhanced spectra from a home-made fast FT system, as mentioned above. An important detail is that to obtain undistorted FT spectra, it is necessary that the complete spectrum to be analyzed is available and reproducible during each acquisition step of the interferometer, which either demands that the OC is steadily locked to the cavity or that it is modulated across a global comb resonance at a sufficiently high repetition rate [98, 122], since for the rest, the stability of the spectral envelope of an OC laser is usually excellent. This detection scheme was also readily exploited in the mid-infrared by the use of a commercial FT spectrometer and femtosecond OPO [123].

Spectral analysis is also possible using multi-heterodyne detection (Fig. 1.8), which delivers an FT interferogram without using moving parts and over short measurement times [114–116]. Two frequency combs with slightly different repetition rates are employed, which corresponds to have a different teeth spacing for the two combs. Thus the gap between closest teeth from both combs may be arranged to be continuously increasing going from one to the other end of the optical spectrum covered by the two combs. When superposing the two laser beams on a fast detector, each pair of teeth gives a beating note at a specific frequency in the radio-frequency domain. The product spectrum of the two optical combs is then directly mapped to a compressed RF spectrum. The principle has been demonstrated with direct absorption spectroscopy by Coddington et al. and Giaccari et al. in 2008 [117, 118] and with a high finesse cavity one year later by Bernhardt et al. [120]. In this demonstration, a first comb is locked to a cavity and the transmitted beam is then mixed with the second comb. The acquisition time for a single frequency scan depends on the mismatch between repetition rates of the two laser combs. Bernhardt et al. achieved

a resolution of 4.5 GHz over 7.5 THz around 1 μm, corresponding to 1500 spectral elements in a recording time of 550 μs.

1.5 Conclusion

In this long introductory chapter we first presented a historical overview of the development of cavity enhanced techniques for absorption spectroscopy in molecular physics, in trace detection and isotope ratio analysis. This overview shows that most forms of CEAS have reached today a good maturity and are fruitful in many domains of application. However, the field is still rich of possibilities to be developed and exploited. In particular, we think that modelocked laser sources present a most promising playing ground.

We then introduced the basic properties of high finesse optical cavities, which are of interest to different forms of CEAS, and which we therefore treated with special attention to some specific details. We also indulged in a detailed consideration of the interaction of different types of laser sources with an optical cavity in view of optimizing injection for CEAS measurements. This has led us to discuss some implementations in more details than others, certainly biased by our own experience.

We leave to the following chapters of this book the task of discussing many more necessary technical details of different aspects of CEAS, from a specialist point of view and with more attention to the applications. We hope this chapter will serve as a sufficiently good starting point for the interested reader who wished to pursue this fascinating subject matter.

Acknowledgements We would like to thank Kevin Lehmann and Marco Prevedelli for their critical reading of the manuscript and the useful discussions concerning several subtle issues.

References

1. G.D. Boyd, J.P. Gordon, Bell Syst. Tech. J. **40**(2), 489 (1961). http://www3.alcatel-lucent.com/bstj/vol40-1961/articles/bstj40-2-489.pdf
2. G.D. Boyd, H. Kogelnik, Bell Syst. Tech. J. **41**(4), 1348 (1962). http://www3.alcatel-lucent.com/bstj/vol41-1962/articles/bstj41-4-1347.pdf
3. D.A. Jackson, Proc. R. Soc. A, Math. Phys. Eng. Sci. **263**(1314), 289 (1961). doi:10.1098/rspa.1961.0161. http://rspa.royalsocietypublishing.org/cgi/doi/10.1098/rspa.1961.0161
4. P. Connes, J. Phys. Radium **19**(3), 262 (1958). doi:10.1051/jphysrad:01958001903026200. http://www.edpsciences.org/10.1051/jphysrad:01958001903026200
5. A. Kastler, Appl. Opt. **1**(1), 17 (1962). doi:10.1364/AO.1.000017
6. A.G. Fox, T. Li, Proc. IEEE **51**(1), 80 (1963). doi:10.1109/PROC.1963.1663. http://ieeexplore.ieee.org/lpdocs/epic03/wrapper.htm?arnumber=1443593
7. H. Kogelnik, T. Li, Proc. IEEE **54**(10), 1312 (1966). doi:10.1109/PROC.1966.5119. http://ieeexplore.ieee.org/lpdocs/epic03/wrapper.htm?arnumber=1447049
8. H. Kogelnik, T. Li, Appl. Opt. **5**(10), 1550 (1966). doi:10.1364/AO.5.001550. http://www.opticsinfobase.org/abstract.cfm?URI=ao-5-10-1550

9. J.A. Arnaud, H. Kogelnik, Appl. Opt. **8**(8), 1687 (1969). doi:10.1364/AO.8.001687. http://www.opticsinfobase.org/abstract.cfm?URI=ao-8-8-1687
10. J.P. Goldsborough, Appl. Opt. **3**(2), 267 (1964). doi:10.1364/AO.3.000267
11. R.L. Fork, D.R. Herriott, H. Kogelnik, Appl. Opt. **3**(12), 1471 (1964). doi:10.1364/AO.3.001471. http://www.opticsinfobase.org/abstract.cfm?URI=ao-3-12-1471
12. G. Rempe, R.J. Thompson, H.J. Kimble, R. Lalezari, Opt. Lett. **17**(5), 363 (1992). http://www.ncbi.nlm.nih.gov/pubmed/19784329
13. R. Damaschini, Opt. Commun. **20**(3), 441 (1977). doi:10.1016/0030-4018(77)90225-5. http://linkinghub.elsevier.com/retrieve/pii/0030401877902255
14. J.M. Herbelin, J.a. McKay, M.a. Kwok, R.H. Ueunten, D.S. Urevig, D.J. Spencer, D.J. Benard, Appl. Opt. **19**(1), 144 (1980). http://www.ncbi.nlm.nih.gov/pubmed/20216808
15. R. Engeln, G. von Helden, G. Berden, G. Meijer, Chem. Phys. Lett. **262**(1–2), 105 (1996). doi:10.1016/0009-2614(96)01048-2. http://linkinghub.elsevier.com/retrieve/pii/0009261496010482
16. J.H. van Helden, D.C. Schram, R. Engeln, Chem. Phys. Lett. **400**(4–6), 320 (2004). doi:10.1016/j.cplett.2004.10.081. http://linkinghub.elsevier.com/retrieve/pii/S0009261404016768
17. D.Z. Anderson, J.C. Frisch, C.S. Masser, Appl. Opt. **23**(8), 1238 (1984). http://www.ncbi.nlm.nih.gov/pubmed/18204709
18. A. Kastler, Nouv. Rev. Opt. **5**(3), 133 (1974). http://iopscience.iop.org/0335-7368/5/3/301
19. J.Y. Lee, J.W. Hahn, Appl. Phys. B, Lasers Opt. **79**(3), 371 (2004). doi:10.1007/s00340-004-1550-2. http://www.springerlink.com/index/10.1007/s00340-004-1550-2
20. T.M. Crawford, in *Southwest Conf. on Optics '85*, ed. by S.C. Stotlar. Proceedings of SPIE, vol. 0540 (1985), pp. 295–302. doi:10.1117/12.976129. http://proceedings.spiedigitallibrary.org/proceeding.aspx?doi=10.1117/12.976129
21. S.N. Jabr, T.M. Crawford, J. Opt. Soc. Am. A **1**(12), 1329 (1984). http://adsabs.harvard.edu/abs/1984JOSAA...1.1329J
22. A. O'Keefe, D.A.G. Deacon, Rev. Sci. Instrum. **59**(12), 2544 (1988). doi:10.1063/1.1139895. http://link.aip.org/link/RSINAK/v59/i12/p2544/s1&Agg=doi
23. D. Romanini, K.K. Lehmann, J. Chem. Phys. **99**(9), 6287 (1993). doi:10.1063/1.465866. http://link.aip.org/link/JCPSA6/v99/i9/p6287/s1&Agg=doi
24. J.J. Scherer, D. Voelkel, D.J. Rakestraw, J.B. Paul, C.P. Collier, R.J. Saykally, A. O'Keefe, Chem. Phys. Lett. **245**(2–3), 273 (1995). doi:10.1016/0009-2614(95)00969-B. http://linkinghub.elsevier.com/retrieve/pii/000926149500969B
25. J.J. Scherer, J.B. Paul, C.P. Collier, R.J. Saykally, J. Chem. Phys. **102**(13), 5190 (1995). doi:10.1063/1.469244. http://link.aip.org/link/JCPSA6/v102/i13/p5190/s1&Agg=doi
26. T. Yu, M.C. Lin, J. Am. Chem. Soc. **115**(10), 4371 (1993). doi:10.1021/ja00063a069 http://pubs.acs.org/doi/abs/10.1021/ja00063a069
27. G. Meijer, M.G.H. Boogaarts, R.T. Jongma, D.H. Parker, A.M. Wodtke, Chem. Phys. Lett. **217**(1–2), 112 (1994). doi:10.1016/0009-2614(93)E1361-J. http://linkinghub.elsevier.com/retrieve/pii/0009261493E1361J
28. P. Zalicki, R.N. Zare, J. Chem. Phys. **102**(7), 2708 (1995). doi:10.1063/1.468647. http://link.aip.org/link/JCPSA6/v102/i7/p2708/s1&Agg=doi
29. J.T. Hodges, J.P. Looney, R.D. van Zee, Appl. Opt. **35**(21), 4112 (1996). doi:10.1364/AO.35.004112. http://www.opticsinfobase.org/abstract.cfm?URI=ao-35-21-4112, http://www.opticsinfobase.org/abstract.cfm?&id=46719
30. K.K. Lehmann, D. Romanini, J. Chem. Phys. **105**(23), 10263 (1996). doi:10.1063/1.472955. http://link.aip.org/link/JCPSA6/v105/i23/p10263/s1&Agg=doi
31. J. Martin, B.A. Paldus, P. Zalicki, E.H. Wahl, T.G. Owano, J.S. Harris, C.H. Kruger, R.N. Zare, Chem. Phys. Lett. **258**(1–2), 63 (1996). doi:10.1016/0009-2614(96)00609-4. http://linkinghub.elsevier.com/retrieve/pii/0009261496006094
32. J.T. Hodges, J.P. Looney, R.D. van Zee, J. Chem. Phys. **105**(23), 10278 (1996). doi:10.1063/1.472956. http://link.aip.org/link/JCPSA6/v105/i23/p10278/s1&Agg=doi

33. R.D. van Zee, J.T. Hodges, J.P. Looney, Appl. Opt. **38**(18), 3951 (1999). http://www.ncbi.nlm.nih.gov/pubmed/18320004
34. D. Romanini, A.A. Kachanov, N. Sadeghi, F. Stoeckel, Chem. Phys. Lett. **264**(3–4), 316 (1997). doi:10.1016/S0009-2614(96)01351-6. http://linkinghub.elsevier.com/retrieve/pii/S0009261496013516
35. D. Romanini, A.A. Kachanov, F. Stoeckel, Chem. Phys. Lett. **270**(5–6), 538 (1997). doi:10.1016/S0009-2614(97)00406-5. http://linkinghub.elsevier.com/retrieve/pii/S0009261497004065
36. D. Romanini, A.A. Kachanov, F. Stoeckel, Chem. Phys. Lett. **270**(5–6), 546 (1997). doi:10.1016/S0009-2614(97)00407-7. http://linkinghub.elsevier.com/retrieve/pii/S0009261497004077
37. R.M. Curran, T.M. Crook, D.J. Zook, MRS Proc. **105**, 175 (1987). doi:10.1557/PROC-105-175
38. B.A. Paldus, C.C. Harb, T.G. Spence, B. Willke, J. Xie, J.S. Harris, R.N. Zare, J. Appl. Phys. **83**(8), 3991 (1998). doi:10.1063/1.367155. http://link.aip.org/link/JAPIAU/v83/i8/p3991/s1&Agg=doi
39. J.T. Hodges, D. Lisak, Appl. Phys. B, Lasers Opt. **85**(2–3), 375 (2006). doi:10.1007/s00340-006-2411-y. http://www.springerlink.com/index/10.1007/s00340-006-2411-y
40. D. Lisak, J.T. Hodges, R. Ciurylo, Phys. Rev. A **73**(1), 1 (2006). doi:10.1103/PhysRevA.73.012507. http://link.aps.org/doi/10.1103/PhysRevA.73.012507
41. G. Giusfredi, S. Bartalini, S. Borri, P. Cancio, I. Galli, D. Mazzotti, P. De Natale, Phys. Rev. Lett. **104**(11), 1 (2010). doi:10.1103/PhysRevLett.104.110801. http://link.aps.org/doi/10.1103/PhysRevLett.104.110801
42. H. Huang, K.K. Lehmann, Opt. Express **15**(14), 8745 (2007). doi:10.1364/OE.15.008745. http://www.ncbi.nlm.nih.gov/pubmed/19547210
43. H. Huang, K.K. Lehmann, Appl. Phys. B, Lasers Opt. **94**(2), 355 (2009). doi:10.1007/s00340-008-3293-y. http://www.springerlink.com/index/10.1007/s00340-008-3293-y
44. H. Huang, K.K. Lehmann, Chem. Phys. Lett. **463**(1–3), 246 (2008). doi:10.1016/j.cplett.2008.08.030. http://linkinghub.elsevier.com/retrieve/pii/S0009261408011081
45. H. Huang, K.K. Lehmann, Appl. Opt. **47**(21), 3817 (2008). doi:10.1364/AO.47.003817. http://www.ncbi.nlm.nih.gov/pubmed/18641751
46. J. Courtois, J.T. Hodges, Opt. Lett. **37**(16), 3354 (2012). doi:10.1364/OL.37.003354. http://www.opticsinfobase.org/abstract.cfm?URI=ol-37-16-3354
47. M. Hippler, M. Quack, Chem. Phys. Lett. **314**(3–4), 273 (1999). doi:10.1016/S0009-2614(99)01071-4. http://linkinghub.elsevier.com/retrieve/pii/S0009261499010714
48. L. Biennier, D. Romanini, A.A. Kachanov, A. Campargue, B. Bussery-Honvault, R. Bacis, J. Chem. Phys. **112**(14), 6309 (2000). doi:10.1063/1.481192. http://link.aip.org/link/JCPSA6/v112/i14/p6309/s1&Agg=doi
49. P. Macko, D. Romanini, S.N. Mikhailenko, O.V. Naumenko, S. Kassi, A. Jenouvrier, V.G. Tyuterev, A. Campargue, J. Mol. Spectrosc. **227**(1), 90 (2004). doi:10.1016/j.jms.2004.05.020. http://linkinghub.elsevier.com/retrieve/pii/S002228520400178X
50. J.W. Hahn, Y.S. Yoo, J.Y. Lee, J.W. Kim, H.W. Lee, Appl. Opt. **38**(9), 1859 (1999). http://www.ncbi.nlm.nih.gov/pubmed/18305817
51. K. An, C. Yang, R.R. Dasari, M.S. Feld, Opt. Lett. **20**(9), 1068 (1995). doi:10.1364/OL.20.001068. http://www.ncbi.nlm.nih.gov/pubmed/19859426, http://www.opticsinfobase.org/abstract.cfm?URI=ol-20-9-1068
52. Y. He, B.J. Orr, Chem. Phys. Lett. **319**(1–2), 131 (2000). doi:10.1016/S0009-2614(00)00107-X. http://linkinghub.elsevier.com/retrieve/pii/S000926140000107X
53. I. Debecker, A.K. Mohamed, D. Romanini, Opt. Express **13**(8), 523 (2005). http://www.opticsinfobase.org/abstract.cfm?URI=OPEX-13-8-2906
54. A. Cygan, D. Lisak, S. Wójtewicz, J. Domyslawska, J.T. Hodges, R. Trawinski, R. Ciurylo, Phys. Rev. A **85**(2), 1 (2012). doi:10.1103/PhysRevA.85.022508

55. M.D. Levenson, B.A. Paldus, T.G. Spence, C.C. Harb, J.S.J. Harris, R.N. Zare, Chem. Phys. Lett. **290**(4–6), 335 (1998). doi:10.1016/S0009-2614(98)00500-4. http://linkinghub.elsevier.com/retrieve/pii/S0009261498005004
56. Y. He, B.J. Orr, Chem. Phys. Lett. **335**(3–4), 215 (2001). doi:10.1016/S0009-2614(01)00031-8. http://linkinghub.elsevier.com/retrieve/pii/S0009261401000318
57. S. Kassi, A. Campargue, J. Chem. Phys. **137**(23), 234201 (2012). doi:10.1063/1.4769974. http://www.ncbi.nlm.nih.gov/pubmed/23267478
58. D. Romanini, P. Dupré, R. Jost, Vib. Spectrosc. **19**(1), 93 (1999). doi:10.1016/S0924-2031(99)00018-1. http://linkinghub.elsevier.com/retrieve/pii/S0924203199000181
59. H. Huang, K.K. Lehmann, Appl. Opt. **49**(8), 1378 (2010). doi:10.1364/AO.49.001378. http://www.opticsinfobase.org/abstract.cfm?URI=ao-49-8-1378
60. I. Galli, S. Bartalini, S. Borri, P. Cancio, D. Mazzotti, P. De Natale, G. Giusfredi, Phys. Rev. Lett. **107**(27), 1 (2011). doi:10.1103/PhysRevLett.107.270802. http://link.aps.org/doi/10.1103/PhysRevLett.107.270802
61. L. Gianfrani, G. Gagliardi, M. van Burgel, E.R.T. Kerstel, Opt. Express **11**(13), 1566 (2003)
62. G. Totschnig, D.S. Baer, J. Wang, Appl. Opt. **39**(12), 2009 (2000). http://www.opticsinfobase.org/abstract.cfm?id=60847
63. R. Engeln, G. Berden, R. Peeters, G. Meijer, Rev. Sci. Instrum. **69**(11), 3763 (1998). doi:10.1063/1.1149176. http://link.aip.org/link/RSINAK/v69/i11/p3763/s1&Agg=doi
64. A. O'Keefe, J.J. Scherer, J.B. Paul, Chem. Phys. Lett. **307**(5–6), 343 (1999). doi:10.1016/S0009-2614(99)00547-3. http://linkinghub.elsevier.com/retrieve/pii/S0009261499005473
65. J.B. Paul, L. Lapson, J.G. Anderson, Appl. Opt. **40**(27), 4904 (2001). http://www.ncbi.nlm.nih.gov/pubmed/18360533
66. D.S. Baer, J.B. Paul, M. Gupta, A. O'Keefe, Appl. Phys. B, Lasers Opt. **75**(2–3), 261 (2002). doi:10.1007/s00340-002-0971-z. http://www.springerlink.com/openurl.asp?genre=article&id=doi:10.1007/s00340-002-0971-z
67. G.S. Engel, W.S. Drisdell, F.N. Keutsch, E.J. Moyer, J.G. Anderson, Appl. Opt. **45**(36), 9221 (2006). http://www.ncbi.nlm.nih.gov/pubmed/17151763newsensitivitylimitsforabsorptionmeasurementsinpassiveopticalcavities.pdf
68. J. Morville, M. Chenevier, A.A. Kachanov, D. Romanini, in *Proceedings of SPIE*, vol. 4485, ed. by A.M. Larar, M.G. Mlynczak (2002), pp. 236–243. doi:10.1117/12.454256
69. J. Morville, D. Romanini, A.A. Kachanov, M. Chenevier, Appl. Phys. B, Lasers Opt. **78**(3–4), 465 (2004). doi:10.1007/s00340-003-1363-8. http://www.springerlink.com/openurl.asp?genre=article&id=doi:10.1007/s00340-003-1363-8
70. J. Morville, S. Kassi, M. Chenevier, D. Romanini, Appl. Phys. B, Lasers Opt. **80**(8), 1027 (2005). doi:10.1007/s00340-005-1828-z. http://www.springerlink.com/index/10.1007/s00340-005-1828-z
71. D. Romanini, M. Chenevier, S. Kassi, M. Schmidt, C. Valant, M. Ramonet, J. Lopez, H.J. Jost, Appl. Phys. B, Lasers Opt. **83**(4), 659 (2006). doi:10.1007/s00340-006-2177-2. http://www.springerlink.com/index/10.1007/s00340-006-2177-2
72. S. Kassi, M. Chenevier, L. Gianfrani, A. Salhi, Y. Rouillard, A. Ouvrard, D. Romanini, Opt. Express **14**(23), 11442 (2006). doi:10.1364/OE.14.011442
73. I. Ventrillard, T. Gonthiez, C. Clerici, D. Romanini, J. Biomed. Opt. **14**(6), 64026 (2009). doi:10.1117/1.3269677. http://www.ncbi.nlm.nih.gov/pubmed/20059264
74. E.R.T. Kerstel, R.Q. Iannone, M. Chenevier, S. Kassi, H.J. Jost, D. Romanini, Appl. Phys. B, Lasers Opt. **85**(2–3), 397 (2006). doi:10.1007/s00340-006-2356-1. http://www.springerlink.com/index/10.1007/s00340-006-2356-1
75. T.J.A. Butler, D. Mellon, J. Kim, J. Litman, A.J. Orr-Ewing, J. Phys. Chem. A **113**(16), 3963 (2009). doi:10.1021/jp810310b
76. V. Motto-Ros, J. Morville, P. Rairoux, Appl. Phys. B, Lasers Opt. **87**(3), 531 (2007). doi:10.1007/s00340-007-2618-6. http://www.springerlink.com/index/10.1007/s00340-007-2618-6

77. V. Motto-Ros, M. Durand, J. Morville, Appl. Phys. B, Lasers Opt. **91**(1), 203 (2008). doi:10.1007/s00340-008-2950-5. http://www.springerlink.com/index/10.1007/s00340-008-2950-5
78. D.J. Hamilton, M.G.D. Nix, S.G. Baran, G. Hancock, A.J. Orr-Ewing, Appl. Phys. B, Lasers Opt. **100**(2), 233 (2009). doi:10.1007/s00340-009-3811-6. http://www.springerlink.com/index/10.1007/s00340-009-3811-6
79. M. Hippler, C. Mohr, K.A. Keen, E.D. McNaghten, J. Chem. Phys. **133**(4), 44308 (2010). doi:10.1063/1.3461061. http://www.ncbi.nlm.nih.gov/pubmed/20687651
80. M. Durand, J. Morville, D. Romanini, Phys. Rev. A **82**(3), 031803(R) (2010). doi:10.1103/PhysRevA.82.031803. http://link.aps.org/doi/10.1103/PhysRevA.82.031803
81. G. Maisons, P. Gorrotxategi Carbajo, M. Carras, D. Romanini, Opt. Lett. **35**(21), 3607 (2010). doi:10.1364/OL.35.003607
82. D.J. Hamilton, A.J. Orr-Ewing, Appl. Phys. B, Lasers Opt. **102**(4), 879 (2010). doi:10.1007/s00340-010-4259-4. http://www.springerlink.com/index/10.1007/s00340-010-4259-4
83. J. Ye, L.S. Ma, J.L. Hall, J. Opt. Soc. Am. B **15**(1), 6 (1998). http://www.opticsinfobase.org/abstract.cfm?id=35318
84. N.J. van Leeuwen, A.C. Wilson, J. Opt. Soc. Am. B **21**(10), 1713 (2004). doi:10.1364/JOSAB.21.001713. http://www.opticsinfobase.org/abstract.cfm?URI=JOSAB-21-10-1713
85. M.S. Taubman, T.L. Myers, B.D. Cannon, R.M. Williams, Spectrochim. Acta, Part A, Mol. Biomol. Spectrosc. **60**(14), 3457 (2004). doi:10.1016/j.saa.2003.12.057. http://www.ncbi.nlm.nih.gov/pubmed/15561632
86. B.M. Siller, M.W. Porambo, A.A. Mills, B.J. McCall, Opt. Express **19**(24), 24822 (2011). http://www.ncbi.nlm.nih.gov/pubmed/22109511
87. F.M. Schmidt, A. Foltynowicz, W. Ma, T. Lock, O. Axner, Opt. Express **15**(17), 10822 (2007). doi:10.1364/OE.15.010822
88. P. Ehlers, I. Silander, J. Wang, O. Axner, J. Opt. Soc. Am. B **29**(6), 1305 (2012). doi:10.1364/JOSAB.29.001305. http://www.opticsinfobase.org/abstract.cfm?URI=josab-29-6-1305
89. P.K. Dasgupta, J.S. Rhee, Anal. Chem. **59**, 783 (1987). http://onlinelibrary.wiley.com/doi/10.1002/cbdv.200490137/abstract, http://pubs.acs.org/doi/abs/10.1021/ac00132a022
90. J.J. Scherer, J.B. Paul, H. Jiao, A. O'Keefe, Appl. Opt. **40**(36), 6725 (2001). http://www.ncbi.nlm.nih.gov/pubmed/18364983
91. S.M. Ball, I.M. Povey, E.G. Norton, R.L. Jones, Chem. Phys. Lett. **342**(1–2), 113 (2001). doi:10.1016/S0009-2614(01)00573-5. http://linkinghub.elsevier.com/retrieve/pii/S0009261401005735
92. S.E. Fiedler, A. Hese, A.A. Ruth, Chem. Phys. Lett. **371**(3–4), 284 (2003). doi:10.1016/S0009-2614(03)00263-X. http://linkinghub.elsevier.com/retrieve/pii/S000926140300263X
93. S.M. Ball, J.M. Langridge, R.L. Jones, Chem. Phys. Lett. **398**(1–3), 68 (2004). doi:10.1016/j.cplett.2004.08.144. http://linkinghub.elsevier.com/retrieve/pii/S0009261404014009
94. P.S. Johnston, K.K. Lehmann, Opt. Express **16**(19), 15013 (2008). http://www.ncbi.nlm.nih.gov/pubmed/18795038
95. S.E. Fiedler, A. Hese, A.A. Ruth, Rev. Sci. Instrum. **76**(2), 23107 (2005). doi:10.1063/1.1841872. http://link.aip.org/link/RSINAK/v76/i2/p023107/s1&Agg=doi
96. G.A. Marcus, H.A. Schwettman, Appl. Opt. **41**(24), 5167 (2002). doi:10.1364/AO.41.005167. http://www.opticsinfobase.org/abstract.cfm?URI=ao-41-24-5167
97. N.R. Newbury, I. Coddington, W.C. Swann, Opt. Express **18**(8), 7929 (2010). http://www.ncbi.nlm.nih.gov/pubmed/20588636
98. R. Grilli, G. Méjean, C. Abd Alrahman, I. Ventrillard, S. Kassi, D. Romanini, Phys. Rev. A **85**(5), 1 (2012). doi:10.1103/PhysRevA.85.051804. http://link.aps.org/doi/10.1103/PhysRevA.85.051804
99. H. Moosmüller, Appl. Opt. **37**(34), 8140 (1998). doi:10.1364/AO.37.008140. http://www.opticsinfobase.org/abstract.cfm?URI=ao-37-34-8140

100. G. Engel, W.B. Yan, J. Dudek, K.K. Lehmann, P. Rabinowitz, in *Laser Spectroscopy XIV International Conference*, ed. by R. Blatt, J. Eschner, D. Leibfried, F. Schmidt-Kaler (World Scientific, Singapore, 1999), pp. 314–315
101. K.K. Lehmann, High-finesse optical resonator for cavity ring-down spectroscopy based upon Brewster's angle prism retroreflectors (1999). http://www.boliven.com/patent/US5973864
102. A.C.R. Pipino, J.W. Hudgens, R.E. Huie, Rev. Sci. Instrum. **68**, 2978 (1997). doi:10.1063/1.1148230
103. T. Udem, J. Reichert, R. Holzwarth, T.W. Hansch, Phys. Rev. Lett. **82**(18), 3568 (1999). doi:10.1103/PhysRevLett.82.3568. http://link.aps.org/doi/10.1103/PhysRevLett.82.3568
104. E.R. Crosson, P. Haar, G.A. Marcus, H.A. Schwettman, B.A. Paldus, T.G. Spence, R.N. Zare, Rev. Sci. Instrum. **70**(1), 4 (1999). doi:10.1063/1.1149533. http://link.aip.org/link/RSINAK/v70/i1/p4/s1&Agg=doi
105. T. Gherman, D. Romanini, Opt. Express **10**(19), 1033 (2002). doi:10.1364/OE.10.001033
106. T. Gherman, E. Eslami, D. Romanini, S. Kassi, J.C. Vial, N. Sadeghi, J. Phys. D, Appl. Phys. **37**(17), 2408 (2004). doi:10.1088/0022-3727/37/17/011. http://stacks.iop.org/0022-3727/37/i=17/a=011?key=crossref.762430055a776caaec8cfaa62362d3df
107. T. Gherman, S. Kassi, A. Campargue, D. Romanini, Chem. Phys. Lett. **383**(3–4), 353 (2004). doi:10.1016/j.cplett.2003.10.148. http://linkinghub.elsevier.com/retrieve/pii/S0009261403019766
108. M.J. Thorpe, K.D. Moll, R. Jason Jones, B. Safdi, J. Ye, Science **311**(5767), 1595 (2006). doi:10.1126/science.1123921. http://www.ncbi.nlm.nih.gov/pubmed/16543457
109. M.J. Thorpe, D. Balslev-Clausen, M.S. Kirchner, J. Ye, Opt. Express **16**(4), 2387 (2008). doi:10.1364/OE.16.002387
110. G. Méjean, R. Grilli, C. Abd Alrahman, I. Ventrillard, S. Kassi, D. Romanini, Appl. Phys. Lett. **100**(25), 251110 (2012). doi:10.1063/1.4726190. http://link.aip.org/link/APPLAB/v100/i25/p251110/s1&Agg=doi
111. R. Grilli, M. Legrand, A. Kukui, G. Méjean, S. Preunkert, D. Romanini, Geophys. Res. Lett. **40** (2013). doi:10.1002/grl.50154
112. C. Gohle, B. Stein, A. Schliesser, T. Udem, T.W. Hansch, Phys. Rev. Lett. **99**(26), 1 (2007). doi:10.1103/PhysRevLett.99.263902. http://link.aps.org/doi/10.1103/PhysRevLett.99.263902
113. M.J. Thorpe, J. Ye, Appl. Phys. B, Lasers Opt. **91**(3–4), 397 (2008). doi:10.1007/s00340-008-3019-1. http://www.springerlink.com/index/10.1007/s00340-008-3019-1
114. S. Schiller, Opt. Lett. **27**(9), 766 (2002). doi:10.1364/OL.27.000766
115. F. Keilmann, C. Gohle, R. Holzwarth, Opt. Lett. **29**(13), 1542 (2004). http://www.ncbi.nlm.nih.gov/pubmed/15259740
116. A. Schliesser, M. Brehm, F. Keilmann, D.W. van der Weide, Opt. Express **13**(22), 9029 (2005). doi:10.1364/OPEX.13.009029
117. I. Coddington, W.C. Swann, N.R. Newbury, Phys. Rev. Lett. **100**(1), 11 (2008). doi:10.1103/PhysRevLett.100.013902. http://link.aps.org/doi/10.1103/PhysRevLett.100.013902
118. P. Giaccari, J.D. Deschênes, P. Saucier, J. Genest, P. Tremblay, Opt. Express **16**(6), 4347 (2008). http://www.ncbi.nlm.nih.gov/pubmed/18542532
119. J.D. Deschênes, P. Giaccari, J. Genest, Opt. Express **18**(22), 23358 (2010). doi:10.1364/OE.18.023358
120. B. Bernhardt, A. Ozawa, P. Jacquet, M. Jacquey, Y. Kobayashi, T. Udem, R. Holzwarth, G. Guelachvili, T.W. Hansch, N. Picqué, Nat. Photonics **4**(1), 55 (2009). doi:10.1038/nphoton.2009.217. http://www.nature.com/nphoton/journal/v4/n1/abs/nphoton.2009.217.html
121. D.W. Chandler, K.E. Strecker, J. Chem. Phys. **136**(15), 154201 (2012). doi:10.1063/1.3700473. http://www.ncbi.nlm.nih.gov/pubmed/22519318
122. S. Kassi, K. Didriche, C. Lauzin, X. de Ghellinck d'Elseghem Vaernewijck, A. Rizopoulos, M. Herman, Spectrochim. Acta, Part A, Mol. Biomol. Spectrosc. **75**(1), 142 (2010). doi:10.1016/j.saa.2009.09.058. http://www.ncbi.nlm.nih.gov/pubmed/19880347

123. X. de Ghellinck d'Elseghem Vaernewijck, K. Didriche, C. Lauzin, A. Rizopoulos, M. Herman, S. Kassi, Mol. Phys. **109**(17–18), 2173 (2011). doi:10.1080/00268976.2011.602990. http://www.tandfonline.com/doi/abs/10.1080/00268976.2011.602990
124. A. Foltynowicz, T. Ban, P. Maslowski, F. Adler, J. Ye, Phys. Rev. Lett. **107**(23), 1 (2011). doi:10.1103/PhysRevLett.107.233002
125. J.J. Scherer, J.B. Paul, A. O'Keefe, R.J. Saykally, Chem. Rev. **97**, 25 (1997). http://pubs.acs.org/doi/abs/10.1021/cr930048d
126. M.D. Wheeler, S.M. Newman, A.J. Orr-Ewing, M.N.R. Ashfold, J. Chem. Soc. Faraday Trans. **94**(3), 337 (1998). doi:10.1039/a707686j. http://xlink.rsc.org/?DOI=a707686j
127. G. Berden, P. Peeters, G. Meijer, Int. Rev. Phys. Chem. **19**(4), 565 (2000). http://www.tandfonline.com/doi/abs/10.1080/01442350750040627#.UjxKi38vQlI
128. G. Berden, G. Meijer, W. Ubachs, in *Experimental Methods in the Physical Sciences*, vol. 40 (Elsevier, Amsterdam, 2003), pp. 47–82. doi:10.1016/S1079-4042(03)80018-8
129. B.A. Paldus, A.A. Kachanov, Can. J. Phys. **83**(10), 975 (2005). doi:10.1139/p05-054. http://www.nrcresearchpress.com/doi/abs/10.1139/p05-054
130. M.I. Mazurenka, A.J. Orr-Ewing, R. Peverall, G.A.D. Ritchie, Annu. Rep. Prog. Chem., Sect. C, Phys. Chem. **101**, 100 (2005). doi:10.1039/b408909j. http://xlink.rsc.org/?DOI=b408909j
131. C. Vallance, New J. Chem. **29**(7), 867 (2005). doi:10.1039/b504628a. http://xlink.rsc.org/?DOI=b504628a
132. K.W. Busch, M.A. Busch, *Cavity-Ringdown Spectroscopy* (American Chemical Society, Washington, 1999), pp. i–vii. doi:10.1021/bk-1999-0720.fw001. http://pubs.acs.org/doi/abs/10.1021/bk-1999-0720.fw001
133. R.D. van Zee, J.P. Looney (eds.), *Experimental Methods in the Physical Sciences*, vol. 40 (Academic Press, New York, 2003), pp. 1–323. doi:10.1016/S1079-4042(03)80015-2. http://www.sciencedirect.com/science/article/pii/S1079404203800152, http://www.sciencedirect.com/science/bookseries/10794042/40
134. G. Berden, R. Engeln, *Cavity Ring-Down Spectroscopy: Techniques and Applications* (Wiley-Blackwell, West Sussex, 2009)
135. S.M. Ball, R.L. Jones, Chem. Rev. **103**(12), 5239 (2003). doi:10.1021/cr020523k. http://www.ncbi.nlm.nih.gov/pubmed/14664650
136. C. Wang, J. Anal. At. Spectrom. **22**(11), 1347 (2007). doi:10.1039/B701223C
137. A. Foltynowicz, F.M. Schmidt, W. Ma, O. Axner, Appl. Phys. B, Lasers Opt. **92**(3), 313 (2008). doi:10.1007/s00340-008-3126-z. <GotoISI>://000258703600003
138. F. Adler, M.J. Thorpe, K.C. Cossel, J. Ye, Annu. Rev. Anal. Chem. **3**, 175 (2010). doi:10.1146/annurev-anchem-060908-155248. http://www.ncbi.nlm.nih.gov/pubmed/20636039
139. A. Foltynowicz, P. Maslowski, T. Ban, F. Adler, K.C. Cossel, T.C. Briles, J. Ye, Faraday Discuss. **150**, 23 (2011). doi:10.1039/c1fd00005e. http://xlink.rsc.org/?DOI=c1fd00005e
140. R.F. Curl, F. Capasso, C. Gmachl, A.A. Kosterev, J.B. McManus, R. Lewicki, M. Pusharsky, G. Wysocki, F.K. Tittel, Chem. Phys. Lett. **487**(1–3), 1 (2010). doi:10.1016/j.cplett.2009.12.073. <GotoISI>://WOS:000274432400001
141. H. Waechter, J. Litman, A.H. Cheung, J.A. Barnes, H.P. Loock, Sensors **10**(3), 1716 (2010). doi:10.3390/s100301716. <GotoISI>://WOS:000277158300016
142. M. Schnippering, S.R.T. Neil, S.R. Mackenzie, P.R. Unwin, Chem. Soc. Rev. **40**(1), 207 (2011). doi:10.1039/c0cs00017e. <GotoISI>://WOS:000285390900016ISI>://000285390900016
143. B.J. Orr, Y. He, Chem. Phys. Lett. **512**(1–3), 1 (2011). doi:10.1016/j.cplett.2011.05.052. http://linkinghub.elsevier.com/retrieve/pii/S0009261411006592
144. D.A. Long, A. Cygan, R.D. van Zee, M. Okumura, C.E. Miller, D. Lisak, J.T. Hodges, Chem. Phys. Lett. **536**, 1 (2012). doi:10.1016/j.cplett.2012.03.035. http://linkinghub.elsevier.com/retrieve/pii/S0009261412003466
145. K.K. Lehmann, H. Huang, in *Frontiers of Molecular Spectroscopy*, ed. by J. Laane (Elsevier, Amsterdam, 2009), pp. 623–658

146. S.S. Brown, Chem. Rev. **103**(12), 5219 (2003). doi:10.1021/cr020645c. http://www.ncbi.nlm.nih.gov/pubmed/14664649
147. M.W. Sigrist, R. Bartlome, D. Marinov, J.M. Rey, D.E. Vogler, H. Wachter, Appl. Phys. B, Lasers Opt. **90**(2), 289 (2008). doi:10.1007/s00340-007-2875-4. <GotoISI>://WOS:000252990900019
148. M.N. Fiddler, I. Begashaw, M.A. Mickens, M.S. Collingwood, Z. Assefa, S. Bililign, Sensors **9**(12), 10447 (2009). doi:10.3390/s91210447. http://www.mdpi.com/1424-8220/9/12/10447, <GotoISI>://WOS:000273048800053
149. X. Cui, C. Lengignon, W. Tao, W. Zhao, G. Wysocki, E. Fertein, C. Coeur, A. Cassez, L. Croize, W. Chen, Y. Wang, W. Zhang, X. Gao, W. Liu, Y. Zhang, F. Dong, J. Quant. Spectrosc. Radiat. Transf. **113**(11), 1300 (2012). http://www.sciencedirect.com/science/article/pii/S0022407311003943
150. D.B. Atkinson, Analyst **128**(2), 117 (2003). doi:10.1039/b206699h. http://xlink.rsc.org/?DOI=b206699h
151. E.R.T. Kerstel, in *Handbook of Stable Isotope Analytical Techniques*, vol. 1, ed. by P.A. De Groot (Elsevier, Amsterdam, 2004), pp. 759–787
152. E.R.T. Kerstel, L. Gianfrani, Appl. Phys. B, Lasers Opt. **92**(3), 439 (2008). doi:10.1007/s00340-008-3128-x. <GotoISI>://000258703600017
153. H.P. Loock, TrAC, Trends Anal. Chem. **25**(7), 655 (2006). doi:10.1016/j.trac.2006.05.003. http://linkinghub.elsevier.com/retrieve/pii/S0165993606001130
154. S. Cheskis, A. Goldman, Prog. Energy Combust. Sci. **35**(4), 365 (2009). doi:10.1016/j.pecs.2009.02.001. <GotoISI>://WOS:000267195600002
155. C.J. Wang, P. Sahay, Sensors **9**(10), 8230 (2009). doi:10.3390/s91008230. <GotoISI>://WOS:000271265800034
156. R.E.H. Miles, S. Rudić, A.J. Orr-Ewing, J.P. Reid, Aerosol Sci. Technol. **45**(11), 1360 (2011). doi:10.1080/02786826.2011.596170. http://dx.doi.org/10.1080/02786826.2011.596170
157. J.S. Caygill, F. Davis, S.P.J. Higson, Talanta **88**, 14 (2012). doi:10.1016/j.talanta.2011.11.043. <GotoISI>://WOS:000301159400002
158. G. Gagliardi, M. Salza, S. Avino, P. Ferraro, P. De Natale, Science (N.Y.) **330**(6007), 1081 (2010). doi:10.1126/science.1195818. http://www.ncbi.nlm.nih.gov/pubmed/21030606
159. A. Yariv, *Quantum Electronics*, 3rd edn. (Wiley, New York, 1989)
160. K.K. Lehmann, in *Cavity-Ringdown Spectroscopy—An Ultratrace-Absorption Measurement Technique*, ed. by K.W. Busch, M.A. Busch (American Chemical Society, Washington, 1999), pp. 106–124. doi:10.1021/bk-1999-0720.ch008. http://pubs.acs.org/doi/abs/10.1021/bk-1999-0720.ch008
161. M. Triki, P. Cermak, G. Méjean, D. Romanini, Appl. Phys. B, Lasers Opt. **91**(1), 195 (2008). doi:10.1007/s00340-008-2958-x. http://www.springerlink.com/index/10.1007/s00340-008-2958-x
162. W.T. Silfast, *Laser Fundamentals*, 1st edn. (Cambridge University Press, New York, 1996)
163. D.R. Herriott, H. Kogelnik, R. Kompfner, Appl. Opt. **3**(4), 523 (1964). doi:10.1364/AO.3.000523. http://www.opticsinfobase.org/abstract.cfm?URI=ao-3-4-523
164. D. Romanini, Modelling the excitation field of an optical resonator. Appl. Phys. B (2013). doi:10.1007/s00340-013-5632-x
165. J. Courtois, A.K. Mohamed, D. Romanini, The degenerate astigmatic cavity. Phys. Rev. A (2013 to appear)
166. W. Riley, *Handbook of Frequency Stability Analysis*, NIST special publication 1065 (1999)
167. P. Werle, R. Miicke, F. Slemr, Appl. Phys., B Photophys. Laser Chem. **57**(2), 131 (1993). doi:10.1007/BF00425997. http://link.springer.com/10.1007/BF00425997
168. P. Werle, Appl. Phys. B **102**(2), 313 (2010). doi:10.1007/s00340-010-4165-9. http://www.springerlink.com/index/10.1007/s00340-010-4165-9
169. L.S. Ma, J.L. Hall, IEEE J. Quantum Electron. **26**(11), 2006 (1990). doi:10.1109/3.62120. http://ieeexplore.ieee.org/lpdocs/epic03/wrapper.htm?arnumber=62120
170. T.W. Hansch, B. Couillaud, Opt. Commun. **35**(3), 441 (1980). doi:10.1016/0030-4018(80)90069-3

171. R.W.P. Drever, J.L. Hall, F.V. Kowalski, J. Hough, G.M. Ford, A.J. Munley, H. Ward, Appl. Phys. B, Lasers Opt. **31**(2), 97 (1983). doi:10.1007/BF00702605. http://www.springerlink.com/index/10.1007/BF00702605
172. D.A. Shaddock, M.B. Gray, D.E. McClelland, Opt. Lett. **24**(21), 1499 (1999). doi:10.1364/OL.24.001499
173. J.L. Hall, M.S. Taubman, J. Ye, Laser stabilization, in *Handbook of Optics, vol. II: Design, Fabrication, and Testing; Sources and Detectors; Radiometry and Photometry*, 3rd edn. (McGraw-Hill, New York, 2010)
174. Z. Li, R.G.T. Bennett, G.E. Stedman, Opt. Commun. **86**(1), 51 (1991). doi:10.1016/0030-4018(91)90242-6. http://linkinghub.elsevier.com/retrieve/pii/0030401891902426
175. Z. Li, G.E. Stedman, H.R. Bilger, Opt. Commun. **100**(1–4), 240 (1993). doi:10.1016/0030-4018(93)90586-T. http://linkinghub.elsevier.com/retrieve/pii/003040189390586T
176. J. Poirson, F. Bretenaker, M. Vallet, A. Le Floch, J. Opt. Soc. Am. B **14**(11), 2811 (1997). doi:10.1364/JOSAB.14.002811. http://www.opticsinfobase.org/abstract.cfm?URI=josab-14-11-2811
177. M.J. Lawrence, B. Willke, M.E. Husman, E.K. Gustafson, R.L. Byer, J. Opt. Soc. Am. B **16**(4), 523 (1999). doi:10.1364/JOSAB.16.000523. http://www.opticsinfobase.org/abstract.cfm?URI=josab-16-4-523
178. J. Morville, D. Romanini, M. Chenevier, A.A. Kachanov, Appl. Opt. **41**(33), 6980 (2002). doi:10.1364/AO.41.006980. http://www.opticsinfobase.org/abstract.cfm?URI=ao-41-33-6980
179. B. Bakowski, L. Corner, G. Hancock, R. Kotchie, R. Peverall, G.A.D. Ritchie, Appl. Phys. B, Lasers Opt. **75**(6–7), 745 (2002). doi:10.1007/s00340-002-1026-1. http://www.springerlink.com/openurl.asp?genre=article&id=doi:10.1007/s00340-002-1026-1
180. Y. He, B.J. Orr, Appl. Phys. B, Lasers Opt. **79**(8), 941 (2004). doi:10.1007/s00340-004-1691-3. http://www.springerlink.com/index/10.1007/s00340-004-1691-3
181. J. Courtois, A.K. Mohamed, D. Romanini, Opt. Express **18**(5), 4845 (2010). http://www.opticsinfobase.org/abstract.cfm?URI=oe-18-5-4845
182. A. Schawlow, C. Townes, Phys. Rev. **112**(6), 1940 (1958). doi:10.1103/PhysRev.112.1940. http://link.aps.org/doi/10.1103/PhysRev.112.1940
183. G. Di Domenico, S. Schilt, P. Thomann, Appl. Opt. **49**(25), 4801 (2010)
184. N. Bucalovic, V. Dolgovskiy, C. Schori, P. Thomann, G. Di Domenico, S. Schilt, Appl. Opt. **51**(20), 4582 (2012). doi:10.1364/AO.51.004582
185. H. Rohde, J. Eschner, F. Schmidt-Kaler, R. Blatt, J. Opt. Soc. Am. B **19**(6), 1425 (2002). doi:10.1364/JOSAB.19.001425. http://www.opticsinfobase.org/abstract.cfm?URI=josab-19-6-1425
186. D. Redding, M. Regehr, L. Sievers, Appl. Opt. **41**(15), 2894 (2002). doi:10.1364/AO.41.002894. http://www.ncbi.nlm.nih.gov/pubmed/12027177
187. J.T. Hodges, J. Looney, R.D. van Zee, Quantitative absorption measurements using cavity-ringdown spectroscopy with pulsed lasers, in *Cavity-Ringdown Spectroscopy. An Ultratrace-Absorption Measurement Technique*, ed. by K.W. Busch, M.A. Busch (American Chemical Society, Washington, 1999). http://pubs.acs.org/isbn/9780841236004
188. D.Z. Anderson, Appl. Opt. **23**(17), 2944 (1984). http://www.ncbi.nlm.nih.gov/pubmed/18213100
189. G. Mueller, Q.Z. Shu, R. Adhikari, D.B. Tanner, D. Reitze, D. Sigg, N. Mavalvala, J. Camp, Opt. Lett. **25**(4), 266 (2000). http://www.ncbi.nlm.nih.gov/pubmed/18059850
190. D.H. Lee, Y. Yoon, E.B. Kim, J.Y. Lee, Y.S. Yoo, J.W. Hahn, Appl. Phys. B, Lasers Opt. **74**(4–5), 435 (2002). doi:10.1007/s003400200802. http://www.springerlink.com/openurl.asp?genre=article&id=doi:10.1007/s003400200802
191. D. Romanini, K.K. Lehmann, J. Chem. Phys. **99**, 6287 (1993). doi:10.1063/1.465866
192. T. Udem, J. Reichert, R. Holzwarth, T.W. Hansch, Opt. Lett. **24**(13), 881 (1999). http://www.ncbi.nlm.nih.gov/pubmed/18073883
193. S.A. Diddams, L.W. Hollberg, L.S. Ma, L. Robertsson, Opt. Lett. **27**(1), 58 (2002). doi:10.1364/OL.27.000058. http://www.opticsinfobase.org/abstract.cfm?URI=ol-27-1-58

194. D.J. Jones, S.A. Diddams, J.K. Ranka, A. Stentz, R.S. Windeler, J.L. Hall, S.T. Cundiff, Science **288**(5466), 635 (2000). doi:10.1126/science.288.5466.635. http://www.sciencemag.org/cgi/doi/10.1126/science.288.5466.635
195. A. Bartels, C.W. Oates, L.W. Hollberg, S.A. Diddams, Opt. Lett. **29**(10), 1081 (2004). doi:10.1364/OL.29.001081. http://www.opticsinfobase.org/abstract.cfm?URI=OL-29-10-1081
196. R. Jason Jones, I. Thomann, J. Ye, Phys. Rev. A **69**(5), 2 (2004). doi:10.1103/PhysRevA.69.051803. http://link.aps.org/doi/10.1103/PhysRevA.69.051803
197. W. Zhang, M. Lours, M. Fischer, R. Holzwarth, G. Santarelli, Y. Le Coq, IEEE Trans. Ultrason. Ferroelectr. Freq. Control **59**(3), 432 (2012). doi:10.1109/TUFFC.2012.2212. http://www.ncbi.nlm.nih.gov/pubmed/22481776
198. J.L. Hall, Rev. Mod. Phys. **78**(4), 1279 (2006). doi:10.1103/RevModPhys.78.1279. http://link.aps.org/doi/10.1103/RevModPhys.78.1279
199. T.W. Hansch, Rev. Mod. Phys. **78**(4), 1297 (2006). doi:10.1103/RevModPhys.78.1297. http://link.aps.org/doi/10.1103/RevModPhys.78.1297
200. T. Gherman, ML-CEAS a new high sensitivity absorption spectroscopy technique using ultra-short laser pulses. Ph.D. thesis, University J. Fourier Grenoble, 2004
201. R. Jason Jones, J.C. Diels, Phys. Rev. Lett. **86**(15), 3288 (2001). doi:10.1103/PhysRevLett.86.3288. http://link.aps.org/doi/10.1103/PhysRevLett.86.3288
202. J.C. Diels, R. Jason Jones, L. Arissian, in *Femtosecond Optical Frequency Comb: Principle, Operation, and Applications*, ed. by J. Ye, S.T. Cundiff (Kluwer Academic/Springer, Norwell, 2005), Chap. 12. http://link.springer.com/chapter/10.1007/0-387-23791-7_12
203. T.C. Briles, D.C. Yost, A. Cingöz, J. Ye, T.R. Schibli, Opt. Express **18**(10), 9739 (2010). doi:10.1364/OE.18.009739. http://www.opticsinfobase.org/abstract.cfm?URI=oe-18-10-9739
204. S. Xiao, A.M. Weiner, Opt. Express **12**(13), 2895 (2004). http://www.ncbi.nlm.nih.gov/pubmed/19483805
205. R. Grilli, G. Méjean, S. Kassi, I. Ventrillard, C. Abd Alrahman, E. Fasci, D. Romanini, Appl. Phys. B, Lasers Opt. **107**(1), 205 (2011). doi:10.1007/s00340-011-4812-9. http://www.springerlink.com/index/10.1007/s00340-011-4812-9
206. S. Xiao, A.M. Weiner, C. Lin, IEEE J. Quantum Electron. **40**(4), 420 (2004). doi:10.1109/JQE.2004.825210. http://ieeexplore.ieee.org/xpls/abs_all.jsp?arnumber=1278611, http://ieeexplore.ieee.org/lpdocs/epic03/wrapper.htm?arnumber=1278611

http://www.springer.com/978-3-642-40002-5

Cavity-Enhanced Spectroscopy and Sensing
Gagliardi, G.; Loock, H.-P. (Eds.)
2014, XIX, 527 p. 206 illus., 97 illus. in color., Hardcover
ISBN: 978-3-642-40002-5